ESOC 2023

The Role of MRI in Stroke Imaging

Brain MRI in an Emergency Department: Clinical Implementation and Experience in the First Year

Vincent Dunet, et al.
Department of Diagnostic and Interventional Radiology, Lausanne University Hospital and University of Lausanne, Switzerland

Updates on Advanced Whole-Brain Vessel Wall Imaging in Stroke Patients

Qi Yang, et al.
Department of Radiology, Beijing Chaoyang Hospital, Capital Medical University, Beijing, China

GOBrain in Acute Neurological Emergencies: Diagnostic Accuracy and Impact on Patient Management

Philipp M. Kazmierczak, et al.
Klinik und Poliklinik für Radiologie, Klinikum der Universität München, Germany

Brain Perfusion Imaging in a Case of Thalamic Stroke: a Clinical Application of 3D Pseudo-Continuous ASL (PCASL)

Fabrizio Esposito, et al.
Department of Medicine, Surgery and Dentistry, Scuola Medica Salernitana, University of Salerno, Baronissi (Salerno), Italy

Ultrafast Brain Imaging with Deep Learning Multi-Shot EPI: Preliminary Clinical Evaluation

John Conklin, et al.
Department of Radiology, Massachusetts General Hospital, Boston, MA, USA

Simultaneous Multi-Slice (Slice Accelerated) Diffusion EPI: Early Experience for Brain Ischemia and Cervical Lymphadenopathy

Val Runge, et al.
Department of Diagnostic, Interventional and Pediatric Radiology, University Hospital of Bern, Inselspital, Bern, Switzerland

SIEMENS Healthineers

Brain MRI in an Emergency Department: Clinical Implementation and Experience in the First Year

Vincent Dunet, M.D.[1]; Chantal Rohner, B.Sc.[1]; David Rodrigues, B.Sc.[1]; Jean-Baptiste Ledoux, B.Sc.[1,2]; Tobias Kober, Ph.D.[1,3]; Philippe Maeder, M.D.[1]; Reto Meuli, M.D.[1]; Sabine Schmidt, M.D.[1]

[1]Department of Diagnostic and Interventional Radiology, Lausanne University Hospital and University of Lausanne, Switzerland.
[2]Center for Biomedical Imaging (CIBM), Lausanne, Switzerland
[3]Advanced Clinical Imaging Technology, Siemens Healthineers, Lausanne, Switzerland

Introduction

While computed tomography (CT) is generally used as a first-line investigation method in emergency departments, magnetic resonance imaging (MRI) is the reference method to accurately detect and characterize cerebral involvement and investigate subtle pathophysiological alterations in most brain diseases, including stroke, seizure, brain tumors, and infections.

Magnetic resonance (MR) investigation for patients referred to emergency departments remains challenging, as scanners are not always available 24/7 and patients are often unstable. Also, as longer acquisition times are needed compared to CT imaging, a strict selection of indications that could benefit from MRI without unnecessarily prolonging the patient workup is mandatory in order to optimize time-to-treatment.

A 3T MAGNETOM Vida scanner (Siemens Healthcare, Erlangen, Germany) was installed in the Emergency Radiological Unit of the Department of Diagnostic and Interventional Radiology of the University Hospital of Lausanne at the end of December 2017 (Fig. 1). To date, this is the first MR scanner located directly within an emergency department in Switzerland. We present brain MR workflow implementation and current brain MR guidelines in the emergency setting. We also report on the activity during the first year of use and results after the first 1,000 brain MR cases.

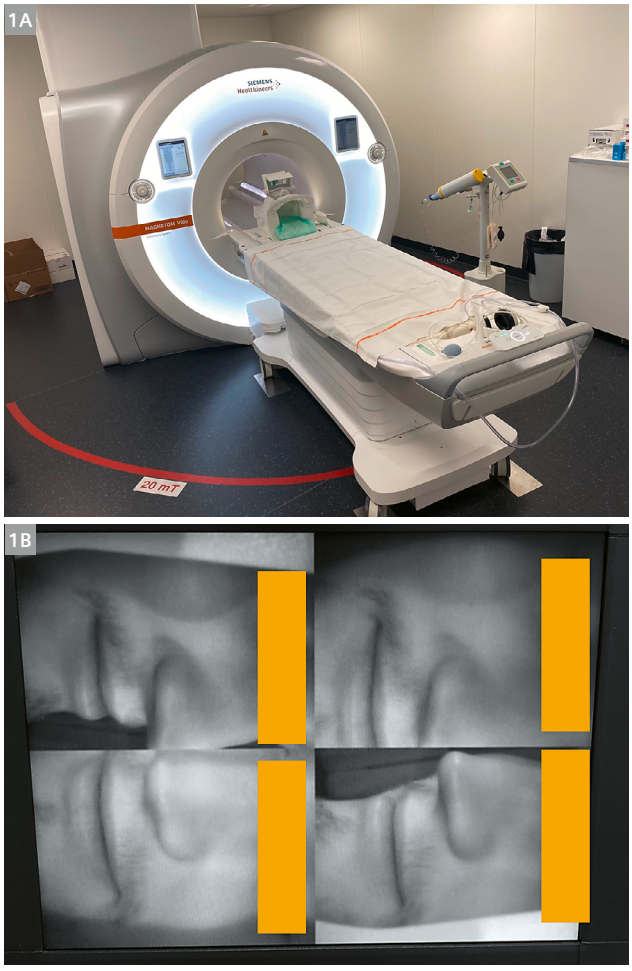

1 3T MAGNETOM Vida scanner and cameras
The 3T MAGNETOM Vida scanner **(1A)** was installed in the Emergency Radiological Unit and was equipped with three cameras: one at the top of the bore and four mounted into the bore **(1B)** to allow monitoring of patients' face and motion on screens in the control room.

MR workflow implementation

MR activity started on January 1, 2018, with 12-hour daily availability until the end of March, followed by 24/7 availability from April 2018. On May 1, 2018 (week 18), we also started using MRI in the 24/7 acute stroke workflow. Emergency department collaborators, including nurses and physicians, were given MR safety information and guidelines on implementing brain MRI both for daily emergency practice as well as for the acute stroke workflow. We also developed a harmonized multi-disciplinary list of indications.

From the beginning, our MR activity was not limited to brain imaging, but also included body imaging for urgent indications for which MRI remains the reference standard, such as the search for bile duct stones.

MR safety

The use of MRI in an emergency setting is a challenge for patient safety and management, so it was necessary to prepare the Emergency Department and Neurology teams. From December 2017 to March 2018, 100 nurses and physicians were given 20 teaching sessions that covered MR setup, safety rules in the MR environment, and MR safety checklists (one for employees, one for patients).

Teaching also included stroke-like workflow simulations, with a volunteer simulating a stroke complicated by an acute seizure that occurred in the MR scanner. Each simulation involved a neuroradiologist, a neurologist, a physician from the Emergency Department, two MR technologists, and two nurses, all blinded for volunteer behavior. Each step was timed, and the availability of materials and respect of MR safety rules were checked by a separate team consisting of one neuroradiologist, one MR technologist, one neurologist, and one physician from the Emergency Department. A debriefing meeting for all participants followed. A second simulation was then conducted to ensure that performance had improved, before making MR available for acute stroke 24/7.

To ensure patient safety during MRI acquisition, EKG, arterial blood pressure, respiratory rate, and oxygen saturation index were continuously monitored on repetition screens in the control room. Furthermore, position, and patients' faces were monitored via dedicated cameras inside the tunnel (Fig. 1).

MR indications and contraindications

A complete switch from CT imaging to MRI is not feasible in an Emergency Department due to the difference in acquisition time, as well as frequent hemodynamic instability and restlessness of admitted patients. It is therefore crucial to determine indications and contraindications in patients that could benefit from a brain MRI.

After multi-disciplinary meetings with the responsible physicians at the Emergency Department (emergency and intensive care physicians, anesthesiologists, neurologists, neurosurgeons), we defined a list of indications for access to MRI within reasonable delay times (Table 1). We also set MR contraindications, including high level of restlessness, hemodynamic or respiratory instability, vomiting, severe claustrophobia, and implanted devices (pacemaker, neurostimulator, cochlear implant, or any fixed head or neck device).

Brain MRI indications and delay	
MRI within 30 min	**MRI within 3 h**
Acute stroke ≤8h with potential IVT or EVT Acute stroke >8h with potential late EVT	Acute coma Meningo-encephalitis Pituitary apoplexia before emergency surgery Brain tumor before emergency decompressive surgery
MRI within 6 h	**No indication for MRI within 6 h**
TIA or acute stroke without IVT or EVT Isolated acute vertigo without any peripheral cause Seizure and refractory status epilepticus Multiple sclerosis and RBON Intracranial hypotension	Any MRI contraindication (CT) Meningitis without focal deficit (CT) Initial workup of an extracerebral tumor without symptoms Acute hemorrhage (angio-CT) Isolated acute headache (angio-CT) Acute brain trauma (CT) Brain tumor with no need for emergency surgery

Table 1: Summary indications for emergency brain MRI and delay.
Abbreviations:
EVT: endovascular thrombectomy
IVT: intravenous thrombolysis
RBON: retrobulbar optical neuritis
TIA: transient ischemic attack

Some patients may have implanted devices but are not able to communicate in emergency situations, for example because of aphasia or cognition problems, so it was decided to perform a chest X-ray before MRI for any unresponsive patient admitted to the Emergency Department without recent documentation in our picture archiving and communication system. This is important especially for patients referred within the context of the acute stroke workflow. The initial evaluation by neurologists includes filling in the patient's safety checklist to decide between CT and MR imaging.

MR protocols

For most emergency cases, MRI is performed with a 64-channel array coil using standard MR protocols, as set up for outpatients; but MR acquisitions in cases of suspected stroke deserve special attention.

Although the choice of CT imaging or MRI does not influence the outcome of patients with acute stroke due to large vessel occlusion [1], MRI is superior to CT imaging for the diagnosis of small ischemic lesions and stroke mimickers [2–4]. However, the use of MRI delays patient management due to longer patient positioning and acquisition time [1], so MR protocols must be optimized. Fast MR sequences reduce acquisition time and the potential impact of patient motion. It is, however, important not to inconsistently reduce the number of MR sequences, and consequently image quality, in order to take advantage of using MRI rather than CT imaging. Given that "time is brain" in a suspected acute stroke, the implementation of MRI needs cautious protocol optimization in order to reduce the "time to therapy". Therapy being intravenous thrombolysis (IVT) and/or endovascular thrombectomy (EVT).

Starting with MR protocols previously used in our institution, we optimized our MR stroke protocol by adapting the number and duration of sequences while keeping optimal spatial resolution (Table 2). The choice following multi-disciplinary discussions was for the "short protocol with 3 mm thick slices and CS-TOF", which represents the best compromise between high image quality, resolution and sequence duration. This protocol was designed for all MRIs performed for suspected acute stroke that could potentially benefit from IVT and/or EVT. Neither the ultra-short protocol nor the short protocol with 5 mm thick slices were chosen because arterial intracranial TOF is necessary for EVT planification, and because thin slices are more suitable for the detection of small infarcts, respectively. Figure 2 summarizes the current workflow for any suspected acute stroke case that may benefit from IVT and EVT.

Sequences	Full protocol	Protocol without suspicion of cervical dissection	Short protocol 3 mm thick slices with CS-TOF	Short protocol 5 mm thick slices with CS-TOF	Ultra-short protocol 3 mm thick slices without TOF
T1_fl2d_sag	1'10	1'10	1'10	0'53	1'10
ep2d_diff_AVC*	1'54	1'54	1'54	1'46	1'54
T2_tse_FLAIR_tra	2'24	2'24	2'24	1'47	2'24
T2_gre_tra_hemo	2'08	2'08	2'08	1'24	2'08
Tof_fl3d_tra_art	6'12	6'12	—	—	—
CS_Tof_fl3d_tra_art	—	—	3'06	3'06	—
T1_space_cor_spair	4'53	—	—	—	—
Angio_fl3d_cor_pre	0'23	0'23	0'23	0'23	0'23
Care_bolus_cor	1'30	1'30	1'30	1'30	1'30
Angio_fl3d_cor_post	0'23	0'23	0'23	0'23	0'23
T1_fl2d_tra	1'05	1'05	1'05	1'05	1'05
ep2d_perf_p3HR	1'45	1'45	1'45	1'45	1'45
Total duration	**23'47**	**18'54**	**15'48**	**14'02**	**12'42**

Table 2: Optimization of brain MRI protocols for acute stroke evaluation.
Abbreviations: CS, Compressed Sensing; FLAIR, fluid attenuated inversion recovery; TOF, time-of-flight.
* Diffusion-weighted imaging is acquired using Simultaneous Multi-Slice acceleration technology.

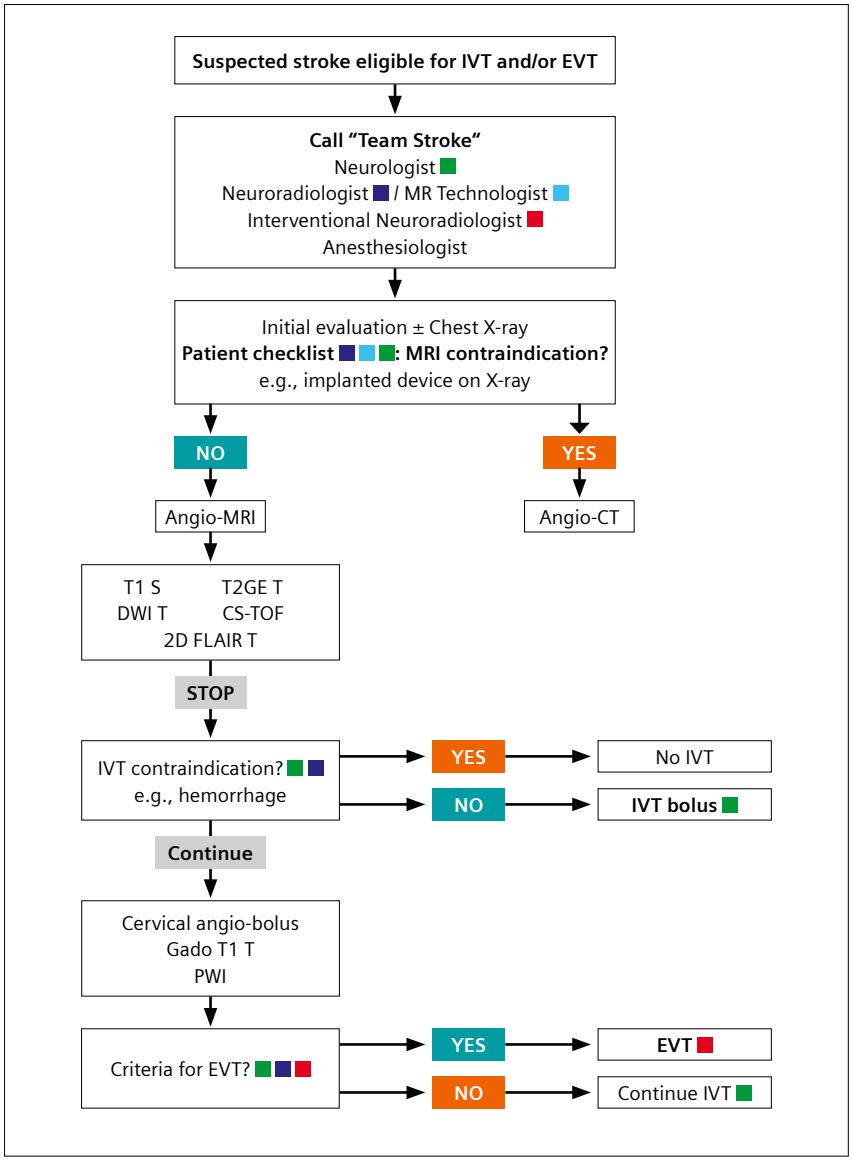

2 **Acute stroke workflow**
Abbreviations:
CS: compressed sensing
DWI: diffusion-weighted imaging
EVT: endovascular thrombectomy
IVT: intravenous thrombolysis
PWI: perfusion weighted imaging
TOF: time-of-flight

Color points represent practitioners involved in the step:
- green for neurologist
- navy blue for neuroradiologist
- cyan for MR technologist
- red for interventional neuroradiologist
- Multiple points are displayed when a multidisciplinary decision is needed.

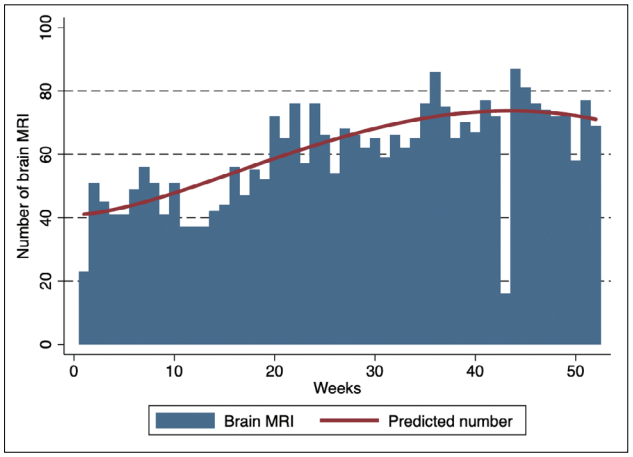

3 Emergency MRI activity over the first year.

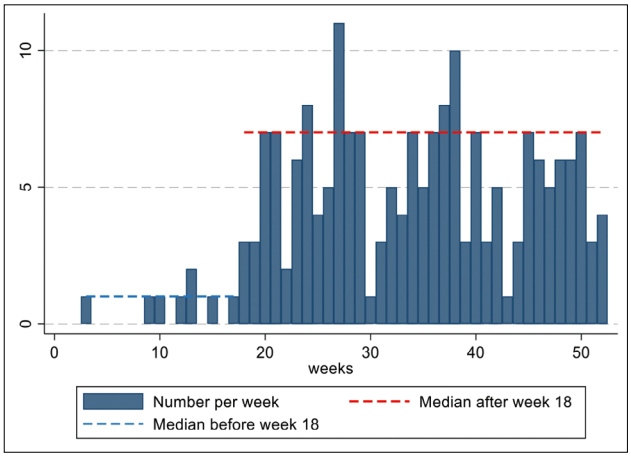

4 Number of brain MRI scans recorded in the Acute Stroke Registry and Analysis of Lausanne.

Experience in the first year

Activity in the first year

Overall, 4,127 MRI exams were performed during the first year. Of these, 3,107 (75%) were brain MRIs. The weekly median number of brain MRIs was 66 (Interquartile range: 55–75, min-max range 16–87). This increased during the first few months from 45 (Interquartile range: 41–51, min-max range 23–56) before week 18, to 70 in the following months (Interquartile range: 65-76, min-max range 16–87). A plateau of 74 was reached at week 35 (i.e. last week of August, median number of brain MRI: 74 per week, interquartile range: 70–77, min-max range 16–87, Fig. 3). This corresponds to a prediction of up to 5,000 MRI scans per year with 24/7 MR scanner availability.

According to the Acute Stroke Registry and Analysis of Lausanne (ASTRAL), the number of patients who underwent a brain MRI at the acute phase of a stroke increased from a median of 1 case per week before week 18 (when the 24/7 acute stroke MRI workflow began) to 7 patients per week thereafter (Fig. 4).

The first 1,000 brain MR examinations: indications, protocols, and results

During the first five months, a total of 1,397 MR examinations were performed, including 1,000 brain MRIs. Of those 1,000 patients, 461 were female and 539 were male, with a median age of 57.2 years (95% interval 42–75 years; range 0–95 years).

Out of these first 1,000 brain MR examinations, 564 were for suspected stroke, 111 for other suspected vascular disease, 51 for seizure, 49 for suspected infection, 177 for known or suspected tumors, 31 for new psychological symptoms, and 17 miscellaneous. A total of 676 included the arterial TOF sequence, and 356 included both the arterial TOF and the cervical angio-bolus sequences.

Overall, 380 brain MRI scans (38%) were determined to be normal. The pathological results were stroke (Fig. 5) in 253 patients (25.3%), other vascular diseases (e.g., aneurysm, venous thrombosis) in 85, acute infection in 60, cerebral tumors in 173, and other miscellaneous diagnoses in 47 patients. MRI acquisition had to be stopped due to intractable nervousness in just two cases. We recorded no major adverse events due to MRI, or side effects after intravenous gadolinium contrast media injection.

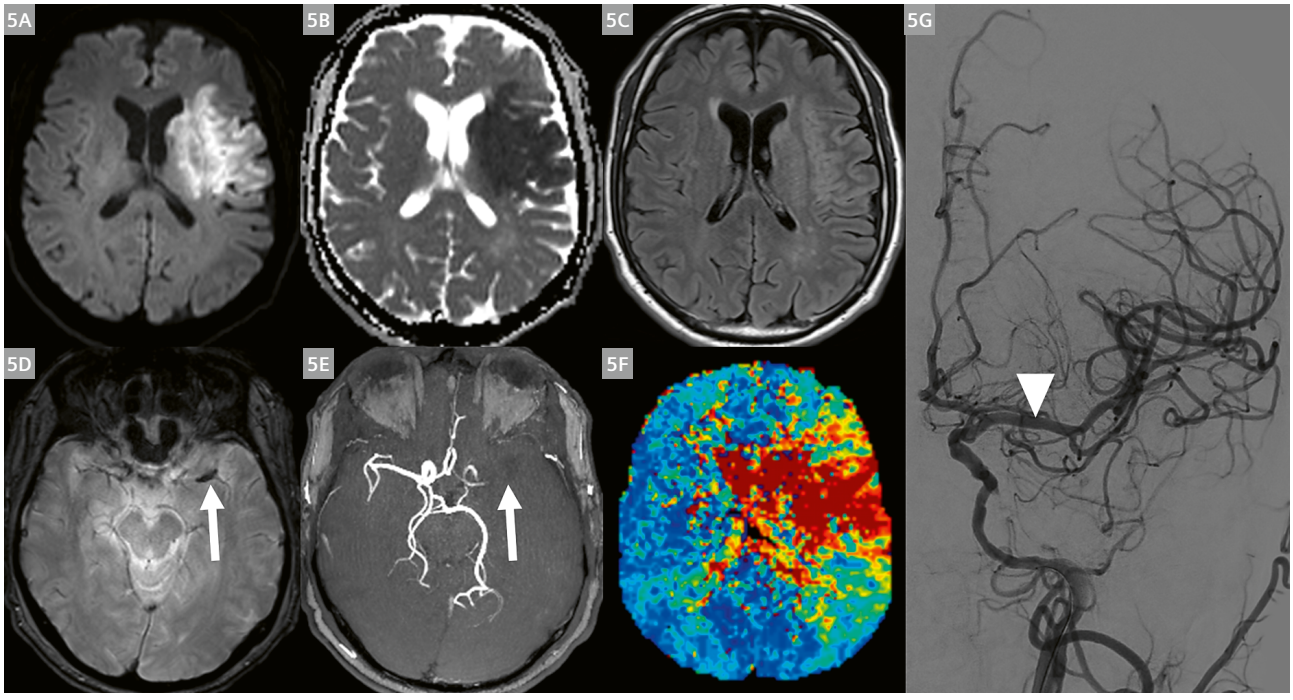

5 **Acute stroke on MRI**
An early acute stroke of the left middle cerebral artery (MCA) is seen as a bright area on the diffusion-weighted image **(5A)**; as an area with low ADC value **(5B)**; and as a faint hyperintense area on FLAIR **(5C)**. The thrombus located within the left MCA appears dark on the T2 gradient echo image **(5D**, arrow) and CS-TOF confirmed vessel occlusion **(5E)**. On perfusion-weighted images, the T_{max} map **(5F)** shows a large area of penumbra surrounding the infarct. The patient consequently underwent intravenous thrombolysis followed by endovascular thrombectomy, with subsequent complete recanalization of the left MCA as seen on end-procedure digital subtraction angiography **(5G**, arrow head).

Discussion

The clinical integration of an MR scanner into an emergency department is feasible. It requires prior teaching of adequate safety rules, multidisciplinary meetings to define the exact indications, and optimization of MR acquisition protocols. When these preliminary conditions are fulfilled, as was achieved in our institution, MRI use could quickly increase up to 5,000 cases per year.

While stroke is the top diagnosis in pathological examinations, we found that 38% of patients admitted to the emergency department with an indication for brain MRI had a normal result. Although the impact on the time of patient discharge from hospital has not yet been assessed, the use of MR in an emergency department could shorten the duration of hospitalization for patients with a normal brain or other MRI.

The true conversion rate from CT imaging to MR examinations should also be evaluated in our institution and in others. Unlike other countries and cities in Switzerland, our department has centralized management of all radiological emergency prescriptions, and a single general radiologist who decides on the imaging modality based on our guidelines. MR activity and conversion from CT imaging to MRI might therefore differ if modalities are managed by multiple practitioners, as is the case in Germany.

References

1 Menjot de Champfleur N, Saver JL, Goyal M, Jahan R, Diener HC, Bonafe A, Levy EI, Pereira VM, Cognard C, Yavagal DR, Albers GW. Efficacy of Stent-Retriever Thrombectomy in Magnetic Resonance Imaging Versus Computed Tomographic Perfusion-Selected Patients in SWIFT PRIME Trial (Solitaire FR With the Intention for Thrombectomy as Primary Endovascular Treatment for Acute Ischemic Stroke). Stroke. 2017;48(6):1560-1566. doi:10.1161/STROKEAHA.117.016669

2 Biesbroek JM, Niesten JM, Dankbaar JW, Biessels GJ, Velthuis BK, Reitsma JB, van der Schaaf IC. Diagnostic accuracy of CT perfusion imaging for detecting acute ischemic stroke: a systematic review and meta-analysis. Cerebrovasc Dis. 2013;35(6):493-501. doi:10.1159/000350200

3 Brazzelli M, Sandercock PA, Chappell FM, Celani MG, Righetti E, Arestis N, Wardlaw JM, Deeks JJ. Magnetic resonance imaging versus computed tomography for detection of acute vascular lesions in patients presenting with stroke symptoms. Cochrane Database Syst Rev. 2009;4:CD007424. doi:10.1002/14651858.CD007424.pub2

4 Schaefer PW, Barak ER, Kamalian S, Gharai LR, Schwamm L, Gonzalez RG, Lev MH. Quantitative assessment of core/penumbra mismatch in acute stroke: CT and MR perfusion imaging are strongly correlated when sufficient brain volume is imaged. Stroke. 2008;39(11):2986-2992. doi:10.1161/STROKEAHA.107.513358

Contact

Dr. Vincent Dunet
Department of Diagnostic and Interventional Radiology
Lausanne University Hospital
Rue du Bugnon 46
CH-1011 Lausanne
Switzerland
Vincent.Dunet@chuv.ch

Updates on Advanced Whole-Brain Vessel Wall Imaging in Stroke Patients

Fang Wu, M.D.[1]; Yuehong Liu, M.D.[2]; Qi Yang, M.D., Ph.D.[2]

[1]Department of Radiology and Nuclear Medicine, Xuanwu Hospital, Capital Medical University, Beijing, China
[2]Department of Radiology, Beijing Chaoyang Hospital, Capital Medical University, Beijing, China

Abstract

Intracranial artery stenosis is one of the common causes of ischemic stroke in Asia. Advances in vessel wall imaging techniques now make it possible to directly visualize the intracranial vessel wall. Several single-center studies have suggested that intracranial vessel wall magnetic resonance imaging (VW-MRI) may provide insights into stroke etiology, vascular pathogenesis, and the risk of recurrent stroke. However, the robustness of intracranial VW-MRI as a valuable tool for the assessment of various cerebrovascular diseases still needs to be validated in a large-scale multicenter study. Thus, our research group initiated a multicenter study in China on February 1, 2017. This study aimed to investigate the clinical utility of whole-brain intracranial VW-MRI in assessing the etiologies in patients with ischemic stroke.

Introduction

Stroke is one of the most common causes of death and disability in the world, which usually causes an abrupt onset of a neurological deficit [1, 2]. Intracranial artery stenosis has been considered a major cause of ischemic stroke, especially in Asia [3]. Traditionally, intracranial vascular diseases have been evaluated with invasive luminal imaging techniques, such as catheter angiography or non-invasive luminal imaging techniques (MR angiography or CT angiography). However, these techniques indirectly visualize vessel wall abnormalities, and many cerebral vasculopathies may have similar luminal narrowing. VW-MRI has been applied as the only non-invasive technique to directly assess the intracranial vessel wall structure [4, 5]. It can provide derived vessel wall characteristics to help clinicians determine stroke etiology, estimate atherosclerotic plaque burden or vasculitis activity, as well as future cerebrovascular events [6].

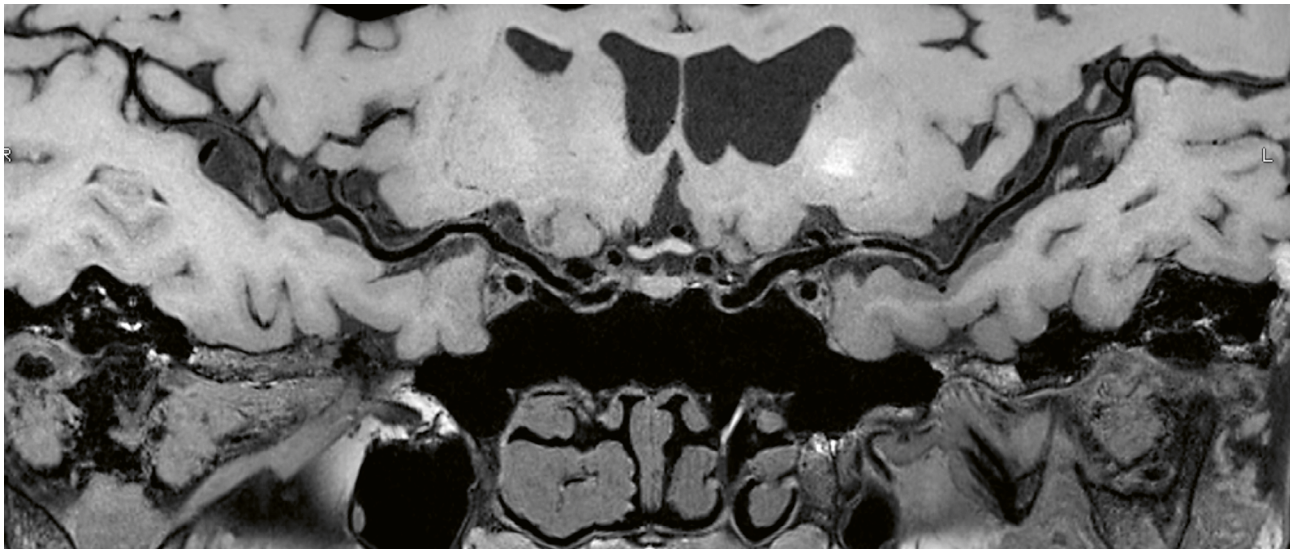

1 Curved-planar reformation of three-dimensional vessel wall magnetic resonance imaging (VW-MRI).

Field strength and pulse sequences

Currently, VW-MRI for intracranial arteries is performed on 3T MRI systems at most centers. Considering the small caliber of intracranial arteries, ultra-high field MRI (7T) may provide an additional value for evaluating intracranial atherosclerotic plaques, as it allows for a high signal-to-noise ratio (SNR), spatial resolution, and contrast-to-noise ratio. Although the feasibility of intracranial VW-MRI at 7T has been demonstrated in several *in-vivo* and *ex-vivo* studies [7, 8], more evidence of additional clinical value of 7T MRI is needed before being used in routine clinical practice. The selection of pulse sequences and protocols remains variable across sites and vendors. To clearly depict the inner and outer boundaries of vessel walls, adequate spatial resolution, as well as excellent blood and cerebrospinal fluid (CSF) suppression are essential for intracranial vessel wall imaging techniques. A two-dimensional (2D) sequence can provide a better in-plane spatial resolution (a voxel size of 0.4 × 0.4 × 2.0 mm^3) for targeted vessel wall lesions. However, it is unable to achieve a more global depiction of multiple vessels and detect lesions without luminal stenosis. Literature shows a shift from 2D to 3D volumetric acquisitions. 3D isotropic imaging with a larger coverage of whole-brain vessels makes it possible to perform multi-planar and curved-planar reformations, as well as assess plaque burden and distribution of major intracranial arteries from various perspectives (Fig. 1) [9]. There are numerous technical developments for VW-MRI pulse sequences aimed to reduce blood and CSF flow artifacts.

Vascular pathologies and their depiction with VW-MRI

The most important recommendation for intracranial VW-MRI in clinical practice is to assess and differentiate intracranial vasculopathies, such as intracranial atherosclerotic plaque, vasculitis, reversible cerebral vasoconstriction syndrome, arterial dissection, and other causes of intracranial arterial narrowing. Diagnosis of cerebrovascular disease has relied on luminal imaging. However, different vasculopathies usually have similar morphological features on luminal imaging. The advent of VW-MRI offers insights into the pathogenesis of cerebrovascular disease. Furthermore, high diagnostic accuracy of VW-MRI for distinguishing a range of vasculopathies has been presented in several studies [4, 10].

Atherosclerotic plaque

VW-MRI of intracranial atherosclerotic plaque typically demonstrates arterial wall thickening, which eccentrically (nonuniformly) involves the circumference of the arterial wall. Intraplaque hemorrhage (IPH), fissured fibrous cap, lipid-rich necrotic core, neovascularization, and inflammation are considered common features of vulnerable plaques and symptomatic lesions. Identification of plaque components with VW-MRI has the potential to identify vulnerable plaque and predict the risk of rupture and events (Fig. 2). For intracranial atherosclerosis, MRI-pathology correlation was explored in limited studies of postmortem artery specimens. Chen et al. reported that

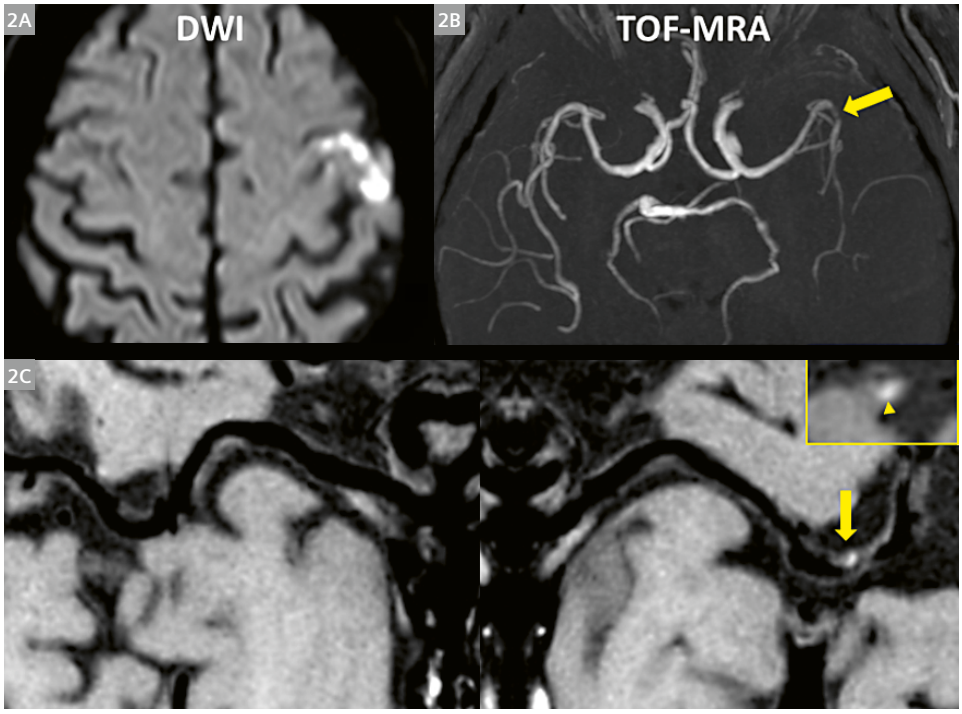

2 70-year-old male patient. **(2A)** Diffusion-weighted imaging (DWI) showed disseminated spotty high signal intensity lesions in the left cortico-subcortical area of the MCA territory; **(2B)** time-of-flight magnetic resonance angiography (TOF-MRA) showed severe stenosis on the relevant MCA (arrow); **(2C)** curved multiplanar reconstruction of pre-contrast VW-MRI showed hyperintense plaque (arrow and arrowhead) on the MCA.

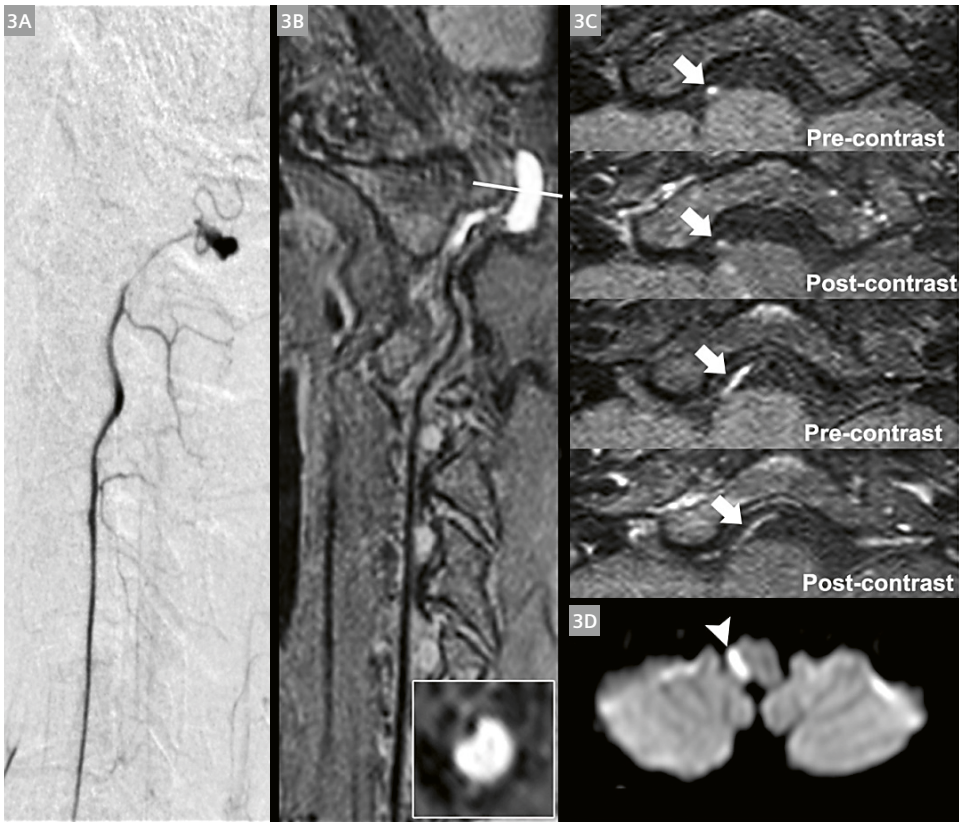

3 A 35-year-old female patient with cervicocranial artery dissection with lateral dorsal medulla syndrome. **(3A)** Digital subtraction angiography showed a severe stenosis and occlusion of the V3-V4 segment of the right vertebral artery; **(3B)** curved planar reformation of VW-MRI demonstrated intramural hematoma (white line) in the vessel wall of the V3 segment of right vertebral artery; **(3C)** axial VW-MRI detected a distal intraluminal thrombus (arrows) without contrast enhancement of the right vertebral artery; **(3D)** DWI showed a single infarction in the right part of the medulla oblongata (arrowhead).

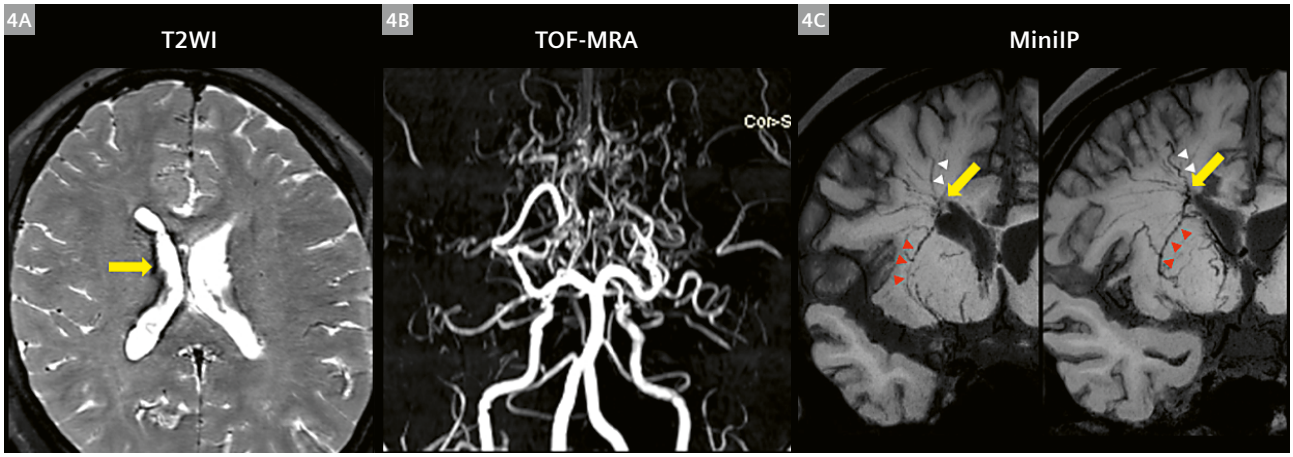

4 A 21-year-old female moyamoya disease patient with right intraventricular hemorrhage. **(4A)** T2-weighted imaging (T2WI) demonstrated that the origin of hemorrhage was in the right periventricular area (yellow arrow); **(4B)** TOF-MRA detected occlusion of bilateral MCAs; **(4C)** minimum intensity projection (MinIP) of VW-MRI revealed an anastomosis (yellow arrow) between the LSAs (red arrowheads) and the medullary arteries (white arrowheads).

high signal on T1-weighted images in specimens at 1.5T was IPH as pathologically-verified in a postmortem case of a Chinese adult [11]. The correlation between the lipid core assessed on histology and low signal on T1-weighted fat-suppressed images within intracranial vessel walls has also been explored [12].

A postmortem study demonstrated that neovasculature can be found in middle cerebral artery (MCA) atherosclerotic plaque and that it was associated with ipsilateral infarction [13]. Gadolinium enhancement of carotid plaques was proven to be associated with vulnerable plaque, neovascularization, macrophages, and loose fibrosis correlating with histopathology [14]. Using VW-MRI, intracranial plaque enhancement can be evaluated and the relationship between plaque enhancement and recent infarction has been established [15].

Arterial dissection

Intracranial arterial dissection most often occurs as an extension of a cervical artery dissection. Simultaneous high-resolution 3D carotid and intracranial imaging has the potential to identify dissected vessels in the head and neck. VW-MRI features of intracranial arterial dissection include a curvilinear hyperintensity on T2-weighted images (intimal flap), separating the true lumen from the false lumen, and crescent-shaped arterial wall thickening with the signal characteristics of blood (intramural hematoma). Early detection of high-risk imaging characteristics of cervicocranial artery dissection may be useful to aid in the preventive treatment of patients with cervicocranial artery dissection without stroke but at higher risk. In a previous study, we investigated the imaging features that are associated with ischemic stroke in patients with cervicocranial artery dissection. We found that the presence of irregular surface and intraluminal thrombus were related to stroke occurrence in these patients (Fig. 3). Integrated head/neck VW-MRI might give insights into the pathogenesis of ischemic stroke in cervicocranial artery dissection. It may be useful for individual prediction of ischemic stroke early in cervicocranial artery dissection [16].

Vasculitis and reversible cerebral vasoconstriction syndrome

VW-MRI often demonstrates smooth and concentric arterial wall thickening and enhancement in patients with central nervous system vasculitis, in comparison with the typical eccentric wall thickening of atherosclerotic plaque. Reversible cerebral vasoconstriction syndrome (RCVS) can also result in concentric arterial wall thickening, but the vessel wall in RCVS is typically nonenhancing (or mildly enhancing) compared with the typical intense wall enhancement in active vasculitis [10]. Early differentiation between vasculitis and RCVS is important: RCVS is treated with observation or calcium channel blockers, whereas vasculitis is treated with steroids and immunosuppressive drugs.

Moyamoya disease

VW-MRI holds significant value in differentiating moyamoya disease and atherosclerotic moyamoya syndrome, which have a significant overlap in luminal morphological patterns. Focal eccentric wall thickening or enhancement was observed in the involved arteries in atherosclerotic moyamoya syndrome, which was different from concentric wall thickening or enhancement in moyamoya disease. Intracranial hemorrhage is one of the most severe complications in patients with moyamoya disease. Moyamoya vessels are the dilated and proliferative perforating arteries serving as collateral circulation, which are more prone to rupture and might be closely associated with intracranial hemorrhage. In a previous study, we investigated the association between dilation, proliferation, and anastomosis of perforating arteries, and intracranial hemorrhage in moyamoya disease patients using VW-MRI. We found that choroidal anastomosis is a valuable imaging biomarker for predicting hemorrhagic events in adult patients with moyamoya disease (Fig. 4). Whole-brain VW-MRI can visualize not only the abnormal collateral vessels but also the anatomy of the parenchymal structure, which may facilitate risk estimates of bleeding in moyamoya disease [17].

Lenticulostriate artery imaging

The lenticulostriate artery (LSA) supplies blood to the basal ganglia and its vicinity in the brain. Impairment of the LSA is associated with ischemic stroke and small-vessel disease. Visualization of the LSA is essential for understanding the mechanisms of microvascular pathologies and potential guiding therapeutic intervention. Using the T1 VW-MRI technique, we have obtained detailed black-blood angiographic delineation of the LSAs [18]. Single subcortical infarctions with a nonstenotic middle cerebral artery have been considered to be caused by lipohyalinosis and fibrinoid degeneration in small-vessel disease, commonly called lacunar strokes. However, large-artery atherothrombosis that blocks the orifice of the perforating artery may also be an important cause of single subcortical infarctions. Jiang et al. used VW-MRI to quantitatively evaluate the associations between the distribution and characteristics of middle cerebral artery plaque and morphological changes to LSAs in the symptomatic and asymptomatic sides of single subcortical infarction patients. They found that superiorly distributed middle cerebral artery plaques at the LSA origin are closely

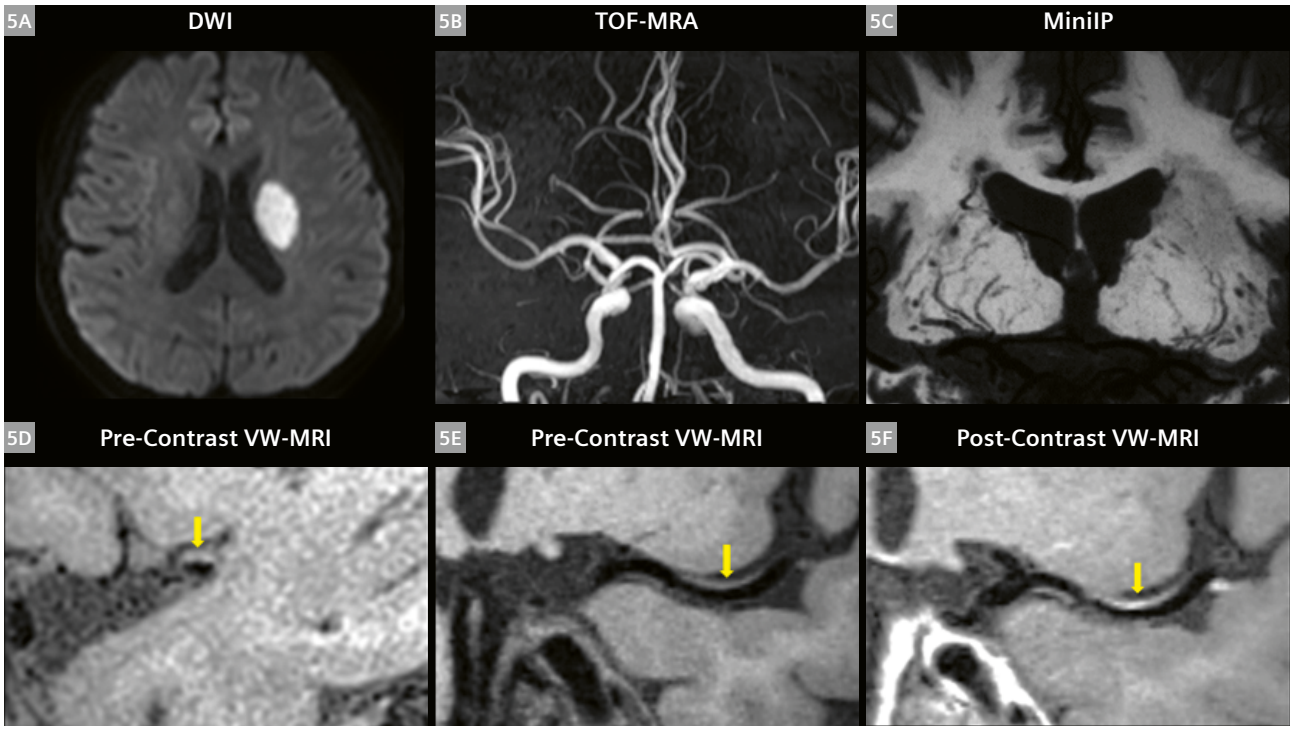

5 A 68-year-old male patient with right limb weakness. **(5A)** DWI showed a single subcortical infarction in the left LSA territory; **(5B)** TOF-MRA showed mild stenosis on the relevant MCA; **(5C)** coronal minimum intensity projection (MinIP) revealed shorter lengths of left lenticulostriate arteries (LSAs) compared with the right side; **(5D)** the cross-section view of pre-contrast VW-MRI demonstrated a superiorly located plaque (arrow) of MCA; **(5E, F)** curved multiplanar reconstruction of pre- and post-contrast VW-MRI showed an isointensity plaque with contrast enhancement (arrow).

associated with morphological changes to the LSA in symptomatic middle cerebral arteries, suggesting that the distribution, rather than the inherent features of plaques, determines the occurrence of single subcortical infarctions (Fig. 5) [19].

Setup of our multicenter study

VW-MRI holds promise of improving our pathological understanding of intracranial artery stenotic disease. The robustness of this technique as a valuable tool for the assessment of various cerebrovascular diseases still needs to be validated in a large-scale multicenter study. We also used the sequence successfully in a multicenter study comprising nine hospitals in China that was initiated by Professor Qi Yang in February 2017. The aim of this study was to accurately classify the etiology of stroke through the scientific research cooperation of various partners, and at the same time carry out early screening and accurate diagnosis of high-risk plaques, thereby providing a new imaging method for the clinical diagnosis and treatment of stroke. The imaging technique used in this project is whole-brain VW-MRI based on sampling perfection with application-optimized contrast using different flip angle evolutions (SPACE) combined with nonselective excitation and a trailing magnetization flip-down module [20, 21]. This imaging technique in combination with a uniform protocol setting on 3T scanners (MAGNETOM Prisma, MAGNETOM Skyra, Siemens Healthcare, Erlangen, Germany) can perform high-resolution imaging of the intracranial vessel wall, clearly depicting the morphology of the vessel wall and distinguishing high-risk vulnerable plaques. In this multi-center study, each participating site carried out imaging studies ranging from intracranial large arterial to perforating arteriole lesions, focusing on cerebrovascular diseases of different etiologies. Several results of this research have been published [22–26].

Outlook

The technology of whole-brain VW-MRI has become a new method for stroke classification. The research performed by our group and other groups presents a first step in designing focused trials on individualized treatment and prevention strategies of intracranial stenosis. Further studies are required to investigate the use of selected biomarkers in randomized control trials of secondary prevention and treatment of intracranial artery stenotic disease.

References

1 GBD 2016 Stroke Collaborators. Global, regional, and national burden of stroke, 1990-2016: a systematic analysis for the Global Burden of Disease Study 2016. Lancet Neurol. 2019;18:439-458.
2 Powers WJ. Acute Ischemic Stroke. N Engl J Med. 2020;383:252-260.
3 Wu S, Wu B, Liu M, et al. Stroke in China: Advances and challenges in epidemiology, prevention, and management. The Lancet. Neurology. 2019;18:394-405.
4 Mandell DM, Matouk CC, Farb RI, et al. Vessel wall MRI to differentiate between reversible cerebral vasoconstriction syndrome and central nervous system vasculitis: Preliminary results. Stroke. 2012;43:860-862.
5 Fan Z, Zhang Z, Chung YC, et al. Carotid arterial wall MRI at 3T using 3D variable-flip-angle turbo spin-echo (TSE) with flow-sensitive dephasing (FSD). J Magn Reson Imaging. 2010;31:645-654.
6 Mandell DM, Mossa-Basha M, Qiao Y, et al. Intracranial vessel wall MRI: Principles and expert consensus recommendations of the American society of neuroradiology. AJNR Am J Neuroradiol. 2017;38:218-229.
7 Harteveld AA, van der Kolk AG, van der Worp HB, et al. High-resolution intracranial vessel wall MRI in an elderly asymptomatic population: comparison of 3T and 7T. Eur Radiol. 2017;27:1585-1595.
8 van der Kolk AG, Zwanenburg JJ, Denswil NP, et al. Imaging the intracranial atherosclerotic vessel wall using 7T MRI: initial comparison with histopathology. AJNR Am J Neuroradiol. 2015;36:694-701.
9 Qiao Y, Guallar E, Suri FK, et al. MR Imaging Measures of Intracranial Atherosclerosis in a Population-based Study. Radiology. 2016;280:860-868.
10 Mossa-Basha M, Shibata DK, Hallam DK, et al. Added value of vessel wall magnetic resonance imaging for differentiation of nonocclusive intracranial vasculopathies. Stroke. 2017;48:3026-3033.
11 Chen XY, Wong KS, Lam WW, et al. High signal on T1 sequence of magnetic resonance imaging confirmed to be intraplaque haemorrhage by histology in middle cerebral artery. Int J Stroke. 2014;9(4):E19.
12 Yang WJ, Chen XY, Zhao HL, et al. Postmortem Study of Validation of Low Signal on Fat-Suppressed T1-Weighted Magnetic Resonance Imaging as Marker of Lipid Core in Middle Cerebral Artery Atherosclerosis. Stroke. 2016;47:2299-2304.
13 Chen XY, Wong KS, Lam WW, et al. Middle cerebral artery atherosclerosis: histological comparison between plaques associated with and not associated with infarct in a postmortem study. Cerebrovasc Dis. 2008;25:74-80.
14 Millon A, Boussel L, Brevet M, et al. Clinical and histological significance of gadolinium enhancement in carotid atherosclerotic plaque. Stroke. 2012;43:3023-3028.
15 Qiao Y, Zeiler SR, Mirbagheri S, et al. Intracranial plaque enhancement in patients with cerebrovascular events on high-spatial-resolution MR images. Radiology. 2014;271:534-542.
16 Wu Y, Wu F, Liu Y, et al. High-Resolution Magnetic Resonance Imaging of Cervicocranial Artery Dissection: Imaging Features Associated With Stroke. Stroke. 2019;50:3101-3107.
17 Wu F, Han C, Liu Y, et al. Validation of Choroidal Anastomosis on High-Resolution Magnetic Resonance Imaging as Imaging Biomarker in Hemorrhagic Moyamoya Disease. Eur Radiol. 2021;31:4548-4556.
18 Zhang Z, Fan Z, Kong Q, et al. Visualization of the lenticulostriate arteries at 3T using black-blood T1-weighted intracranial vessel wall imaging: comparison with 7T TOF-MRA. Eur Radiol. 2019;29:1452-1459.
19 Jiang S, Yan Y, Yang T, et al. Plaque Distribution Correlates With Morphology of Lenticulostriate Arteries in Single Subcortical Infarctions. Stroke. 2020;51:2801-2809.
20 Fan Z, Yang Q, Deng Z, et al. Whole-brain intracranial vessel wall imaging at 3 Tesla using cerebrospinal fluid-attenuated T1-weighted 3D turbo spin echo. Magn Reson Med. 2017;77:1142–1150.
21 Yang Q, Deng Z, Bi X, et al. Wholebrain vessel wall MRI: a parameter tune-up solution to improve the scan effciency of three-dimensional variable flip-angle turbo spin-echo. J Magn Reson Imaging. 2017;46:751–757.
22 Liu Y, Li S, Wu Y, et al. The Added Value of Vessel Wall MRI in the Detection of Intraluminal Thrombus in Patients Suspected of Craniocervical Artery Dissection. Aging & Dis.2021; Doi:10.14336/AD.2021.0502.
23 Jiang S, Yan Y, Yang T, et al. Plaque Distribution Correlates With Morphology of Lenticulostriate Arteries in Single Subcortical Infarctions. Stroke. 2020;51(9):2801-2809.
24 Wu Y, Wu F, Liu Y, Yang Q, et al. High-Resolution Magnetic Resonance Imaging of Cervicocranial Artery Dissection: Imaging Features Associated with Stroke. Stroke. 2019; 50(11):3101-3107.
25 Wu F, Ma Q, Song H, et al. Differential Features of Culprit Intracranial Atherosclerotic Lesions: A Whole-Brain Vessel Wall Imaging Study in Patients With Acute Ischemic Stroke. J Am Heart Assoc. 2018 Jul 22;7(15).
26 Wu F, Song H, Ma Q, et al. Hyperintense plaque on intracranial vessel wall magnetic resonance imaging as a predictor of artery-to-artery embolic infarction. Stroke. 2018; 49(4):905-911.

Contact

Professor Qi Yang, M.D., Ph.D.
Vice Chair
Department of Radiology
Beijing Chaoyang Hospital
Capital Medical University
No. 8 Gongti South Road
Chaoyang District
Beijing 100020, China
Phone: +86 (0) 10-8523-1928
yangyangqiqi@gmail.com

GOBrain in Acute Neurological Emergencies: Diagnostic Accuracy and Impact on Patient Management

Philipp M. Kazmierczak, M.D.[1]; Max Dührsen, MS[1]; Robert Forbrig, M.D.[2]; Maximilian Patzig, M.D.[2]; Matthias Klein, M.D.[3]; Andreas Pomschar, M.D.[4]; Wolfgang G. Kunz, M.D.[1]; Daniel Puhr-Westerheide, M.D.[1]; Jens Ricke, M.D.[1]; Olga Solyanik, M.D.[1]*; Clemens C. Cyran, M.D.[1,4]*

***Olga Solyanik and Clemens C. Cyran contributed equally and share last authorship.**

[1]Klinik und Poliklinik für Radiologie, Klinikum der Universität München, Germany
[2]Institut für Neuroradiologie, Klinikum der Universität München, Germany
[3]Neurologische Klinik und Poliklinik, Klinikum der Universität München, Germany
[4]DIE RADIOLOGIE, München, Germany

Introduction

Even though computed tomography (CT) of the head is the primary imaging modality used in the majority of institutions to rule out intracranial pathologies in acute neurological emergencies, magnetic resonance imaging (MRI) remains the imaging reference standard for the detection and differential diagnosis of intracranial lesions. However, the use of MRI in the acute setting is still limited by long acquisition times for multi-sequence protocols. This drawback may now be overcome by a novel ultra-fast brain MRI protocol, which allows for the acquisition of five standard sequences in just 04:33 min (GOBrain, Siemens Healthcare, Erlangen, Germany, optimized for use in our institution, including sagittal T1-weighted gradient echo (GRE), axial T2-weighted turbo spin echo (TSE), axial T2-weighted TSE fluid-attenuated inversion recovery (FLAIR), axial diffusion-weighted (DWI) single-shot echo-planar imaging (EPI), axial T2*-weighted EPI-GRE). To validate the GOBrain protocol for use in the emergency setting, we hypothesized that

a. image quality and diagnostic performance of GOBrain for the detection of intracranial pathologies are non-inferior to the standard-length brain MRI protocol,
b. GOBrain leads to a change in patient management compared to CT alone.

Sequences		Image Quality						GWM Differentiation			
		Scores						Scores			
		1	2	3	4	5	Median	0	1	2	Median
T1-weighted	Conventional	0	0	1	58	0	4	0	6	53	2
	GOBrain	0	0	0	59	0	4	0	7	52	2
T2-weighted	Conventional	0	0	3	54	2	4	0	34	25	1
	GOBrain	0	0	2	57	0	4	0	39	20	1
FLAIR	Conventional	0	0	2	56	1	4	0	32	27	1
	GOBrain	0	0	1	58	0	4	0	31	28	1
DWI	Conventional	0	0	0	59	0	4	NA	NA	NA	NA
	GOBrain	0	0	0	59	0	4	NA	NA	NA	NA
T2*	Conventional	0	0	6	53	0	4	NA	NA	NA	NA
	GOBrain	0	2	56	1	0	3	NA	NA	NA	NA

Table 1: Image quality assessments (consensus reading). NA = not applicable; GWM = gray-white matter.

Materials and methods

A total of 449 consecutive patients presenting to our emergency department with acute non-traumatic neurological symptoms were evaluated [1]. Of these, 238 patients underwent a head CT scan to exclude an intracranial pathology. In case of a negative head CT scan, patients were included in this prospective single-center trial and were transferred to the 3T MRI suite (MAGNETOM Skyra, Siemens Healthcare, Erlangen, Germany). A total of 60 patients (30 female, 30 male; mean age 61 years) were successfully included. The MRI examinations were performed using a 20-channel receiver head coil.
Two brain MRI protocols (GOBrain and a standard-length protocol serving as reference standard) including the following five non-contrast standard sequences were acquired in randomized order:

1. **Sagittal T1-weighted GRE**
   (GOBrain 00:41 min; standard-length: 01:34 min)
2. **Axial T2-weighted TSE**
   (GOBrain 01:02 min; standard-length: 03:45 min)
3. **Axial T2-weighted TSE FLAIR**
   (GOBrain 01:52 min; standard-length: 04:02 min)
4. **Axial T2*-weighted EPI-GRE**
   (GOBrain 00:06 min; standard-length: 04:44 min)
5. **Axial DWI SS-EPI**
   (GOBrain 00:38 min; standard-length: 01:06 min)

Total acquisition times: GOBrain 04:19 min, standard-length protocol 15:11 min, localizer 00:14 min (same for both protocols). Two blinded board-certified neuroradiologists independently analyzed the image datasets with regard to overall image quality (5-point Likert scale: 1 – non-diagnostic, 2 – substantial artifacts, 3 – satisfactory, 4 – minor artifacts, 5 – no artifacts) and gray-white matter differentiation as a surrogate of image quality (T1-weighted, T2-weighted, and FLAIR images; 0 = no visible gray-white matter differentiation, 1 = unclear but recognizable borders, 2 = clear differentiation) [2]. In case of divergent results, a consensus reading was performed by a third reader. To calculate the parameters of diagnostic accuracy for the GOBrain protocol, image datasets were read regarding six defined intracranial pathology categories: acute ischemia, chronic infarction, intracranial hemorrhage/microbleeds, edema, white matter lesion, and miscellaneous. A consensus reading was performed in case of divergent reading results. Due to severe motion artifacts, one patient was excluded and 59 patients were successfully included in the statistical analysis.

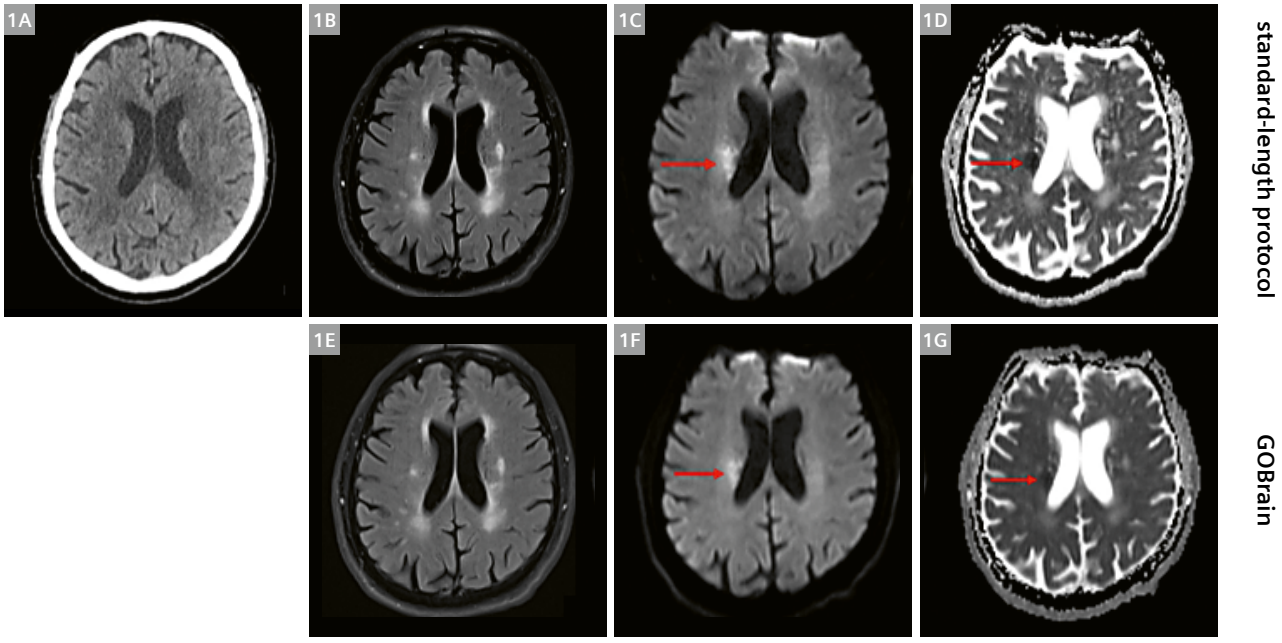

1 **CT-occult acute ischemia (right corona radiata).** Axial non-contrast head CT scan **(1A)**, FLAIR **(1B, E)**, DWI **(1C, F)**, ADC map **(1D, H)** from the standard-length protocol (top row) and GOBrain (bottom row) in a 72-year-old man presenting with acute left facial paralysis, dysarthria, and left-body coordination disorder. No evidence of ischemia or hemorrhage on non-contrast CT. MRI revealed an acute ischemia in the right internal capsule and the corona radiata (red arrow). Note the equivalent image quality and lesion conspicuity of both protocols.

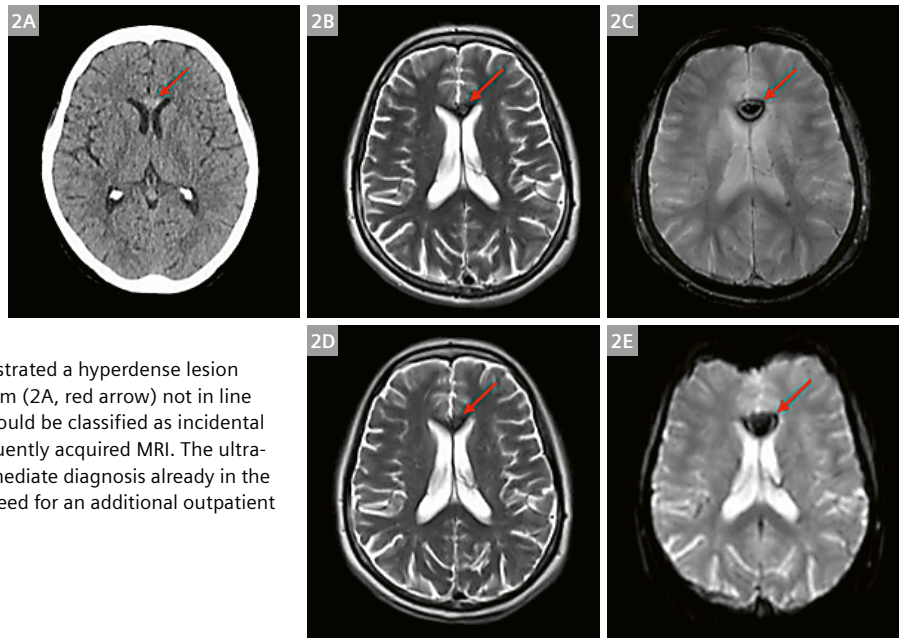

2 Incidental cavernoma (genu of the corpus callosum). Axial non-contrast head CT scan **(2A)**, axial T2 TSE **(2B, D)**, axial T2* **(2C, E)** from the standard-length protocol (top row) and GOBrain (bottom row) of a 62-year-old woman reporting temporary visual disturbance in the right eye. No correlation of the symptoms in both imaging modalities. However, non-contrast CT imaging demonstrated a hyperdense lesion in the genu of the corpus callosum (2A, red arrow) not in line with acute hemorrhage, which could be classified as incidental cavernoma based on the subsequently acquired MRI. The ultra-fast MRI protocol enabled an immediate diagnosis already in the emergency setting without the need for an additional outpatient MRI scan a few days later.

Results

Image quality of the GOBrain protocol was equivalent to the standard-length protocol: Results of image quality and gray-white matter differentiation assessments are listed in Table 1. Compared to CT imaging, 93 additional intracranial lesions were detected using the ultra-fast protocol (n = 21 acute ischemia, n = 27 intracranial hemorrhage/microbleeds, n = 2 edema, n = 38 white matter lesion, n = 3 chronic infarction, n = 2 others) while 101 additional intracranial lesions were detected using the standard-length protocol (n = 24 acute ischemia, n = 32 intracranial hemorrhage/microbleeds, n = 2 edema, n = 38 white matter lesion, n = 3 chronic infarction, n = 2 others). GOBrain demonstrated high diagnostic accuracy in detecting intracranial pathologies, with a sensitivity of 0.939 (95% CI: 0.881; 0.972) and a specificity of 1.000 (95% CI: 0.895; 1.000). Figures 1 and 2 demonstrate representative clinical cases in which GOBrain proved to be equivalent to the standard-length protocol reference standard. A change in patient management based on the MRI was noted in 10% (6/59; admission to a dedicated stroke unit in 6/59 patients, initiation of acetyl-salicylic acid treatment in 3/6 stroke unit patients).

Discussion

In this prospective study, we investigated a novel ultra-fast (04:33 min/5 sequences) brain MRI protocol in the neurological emergency setting. Image quality and diagnostic performance of the GOBrain protocol demonstrated to be non-inferior to a standard-length brain MRI protocol. Furthermore, MRI led to a change in patient management in 10% of cases compared to CT imaging alone. Our data provide evidence for the standard use of the ultra-fast GOBrain protocol as a valid alternative to CT imaging for the detection and differential diagnosis of intracranial pathologies in selected acute neurological emergency patients. The ultra-fast MRI protocol may be individualized by adding sequences, such as dedicated brain stem DWI or constructive interference in steady state (CISS) sequences for optimized diagnosis of infratentorial pathologies, a contrast-enhanced T1-weighted sequence for suspected tumor or neuroinflammatory disease, or MR angiography to exclude vascular pathologies.

Contact

PD Dr. med. Philipp M. Kazmierczak, MD
Klinik und Poliklinik für Radiologie
Klinikum der Universität München
Marchioninistr. 15
81377 München
Germany
Tel.: +49 89 4400 73620
Fax: +49 89 4400 78832
philipp.kazmierczak@med.uni-muenchen.de

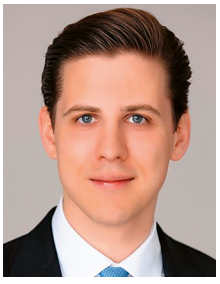

References

1 Kazmierczak PM, Dührsen M, Forbrig R, et al. Ultrafast Brain Magnetic Resonance Imaging in Acute Neurological Emergencies: Diagnostic Accuracy and Impact on Patient Management. Invest Radiol 2020;55:181-189.
2 Prakkamakul S, Witzel T, Huang S, et al. Ultrafast Brain MRI: Clinical Deployment and Comparison to Coventional Brain MRI at 3T. J Neuroimaging 2016;26:503-510.

The Role of Imaging within the Stroke Care Pathway

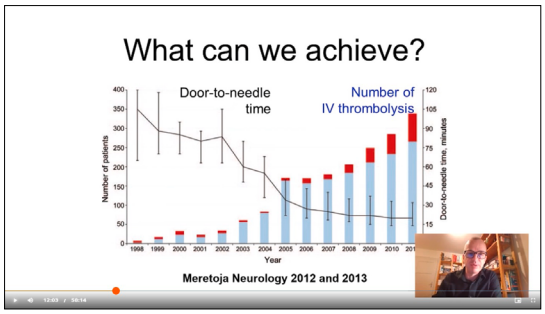

Stroke as an Interdisciplinary Disease. The View of the Neurologist

Urs Fischer, M.D.
Dept. of Neurology, University Hospital Bern,
Inselspital Bern, Switzerland

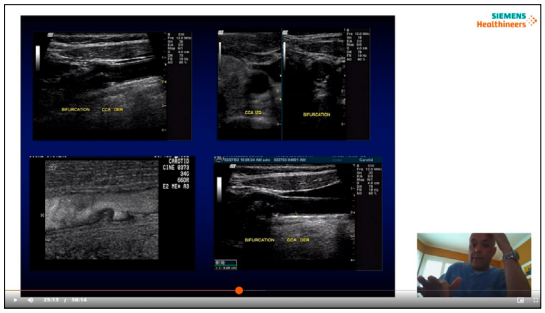

Role of Carotid Doppler in Stroke

Jorge Luis Sarmiento G., M.D.
Professional Radiology, El Paso, TX, USA

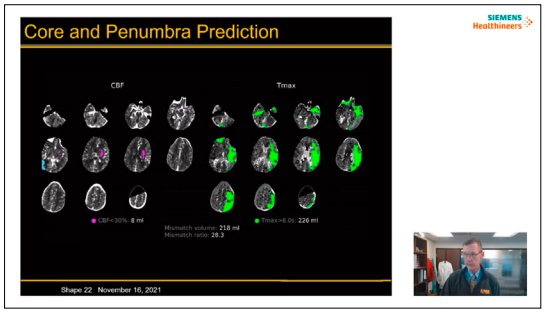

The Role of CT within the Stroke Care Pathway

Colin P. Derdeyn, M.D.
Iowa Institute of Biomedical Imaging;
University of Iowa Hospitals and Clinics, Iowa City, IA, USA

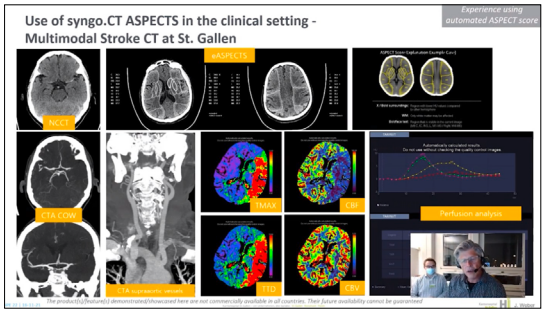

Experience Using Automated ASPECT Score

Johannes Weber, M.D. and Damian Koller
Kantonsspital St. Gallen, Switzerland

Listen to the talks at

https://events.siemens-healthineers.com/sessions/customer-talk/the-role-of-imaging-within-the-stroke-care-pathway

Brain Perfusion Imaging in a Case of Thalamic Stroke: a Clinical Application of 3D Pseudo-Continuous ASL (PCASL)

Renzo Manara[1,2]; Josef Pfeuffer[3]; Fabrizio Esposito[1,2]

[1]Department of Medicine, Surgery and Dentistry, Scuola Medica Salernitana, University of Salerno, Baronissi (Salerno), Italy
[2]Department of Diagnostic Imaging, University Hospital San Giovanni di Dio e Ruggi D'Aragona, Scuola Medica Salernitana, Salerno, Italy
[3]Siemens Healthcare GmbH, MR Application Development, Erlangen, Germany

Abstract

Brain perfusion MRI can help us better understand and monitor the metabolic and functional correlates of a stroke lesion, both in the acute and chronic phase and beyond the local tissue damage. Arterial spin labeling (ASL) allows repeated perfusion measurements and quantifications of cerebral blood flow (CBF) over the whole brain without the need for exogenous contrast. When it comes to monitoring stroke patients, ASL can therefore provide useful information about the short-term (dynamic) or long-term (e.g., chronic vs. acute) effects of pharmacological treatments or surgical interventions with respect to stroke onset.

Here we report a case of thalamic stroke where the relationship between the whole-brain CBF pattern and the tissue outcome is illustrated in the subacute and chronic phases, before and after five months of pharmacological treatment, by co-registering CBF maps from 3D pseudo-continuous ASL (3D PCASL)[1] images and T2-weighted fluid-attenuated inversion recovery

[1]*WIP, the product is currently under development and is not for sale in the US and in other countries. Its future availability cannot be ensured.*

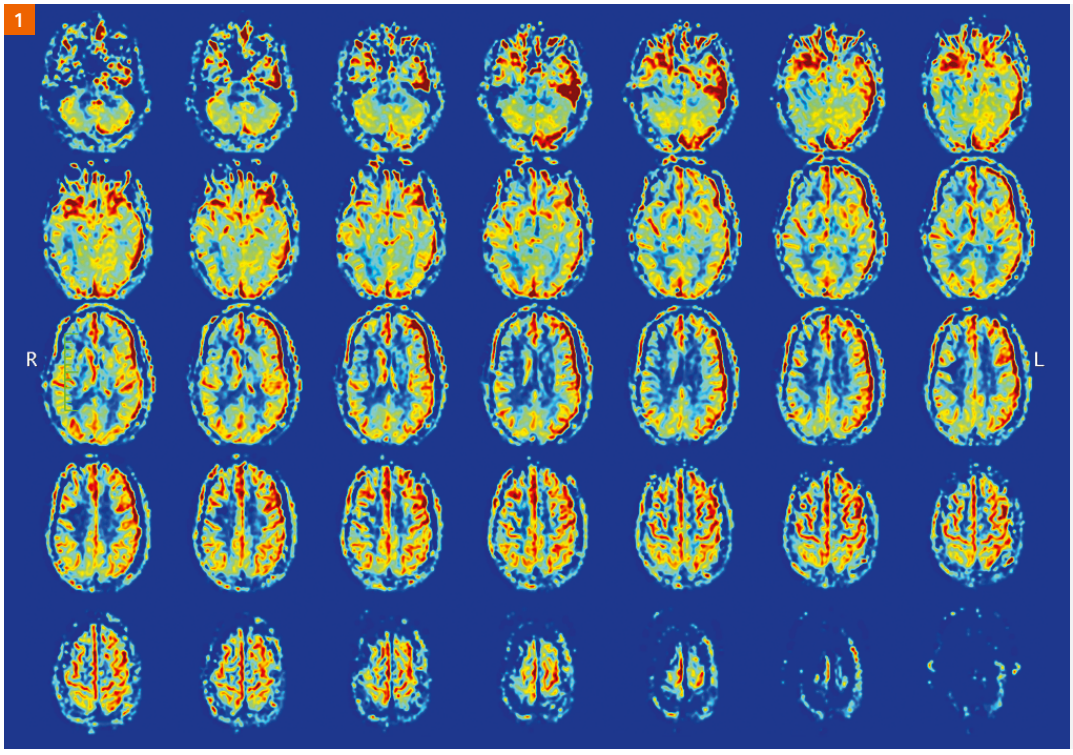

Figure 1: rCBF map (mL / 100 g / min) of a 31-year-old woman with a stenosis of the distal basilar artery, acquired in the subacute phase using 3D PCASL. The color map "jet" (blue/green: low perfusion, yellow/red: high perfusion) was used to map the image values.

(3D FLAIR) images. We compare these to conventional magnetic resonance angiography (MRA) images.

Visualizing changes in perfusion patterns provided significant information that could not be easily produced with conventional non-invasive MRI techniques, and might therefore provide new insight into the functional, vascular, and neuronal changes that follow an ischemic brain injury. If introduced to a routine clinical setting, 3D PCASL could certainly allow the non-invasive and rapid collation of quantitative parameters that might be useful predictors of outcome. It could also provide a deeper understanding of metabolic and vascular phenomena caused by cerebro-afferent vessel occlusion, and therefore help improve tailored approaches to ischemic stroke.

Introduction

Monitoring brain perfusion helps us to understand the metabolic and functional correlates of both acute and chronic cerebrovascular lesions in a way that goes beyond the local tissue damage associated with the structural lesion. Compared to dynamic susceptibility contrast (DSC), arterial spin labeling (ASL) allows repeat perfusion measurements within a few hours and over weeks or months. It also provides absolute quantifications of cerebral blood flow (CBF) across the entire brain without the need for exogenous contrast [1]. When it comes to managing patients with acute stroke, ASL can therefore provide useful information about the short-term (dynamic) or long-term (e.g., chronic vs acute) effects of pharmaco-logical treatments or surgical interventions [2]. Among the different ASL implementations on clinical MRI scanners, pseudo-continuous 3D ASL[1] is recommended by the ISMRM Perfusion Study Group as the method of choice for clinical imaging [3].

Here we report on a patient with vertebrobasilar stroke caused by spontaneous basilar artery vasospasm. We illustrate the relationship between the whole-brain CBF pattern and the narrowing of the intracranial artery in the subacute phase, and show the tissue outcome and the consequences of ischemia in strategic brain regions (hippocampus and thalamus) after five months of pharmacological treatment. In particular, we postprocessed ASL images obtained with a prototype version of the 3D pseudo-continuous ASL (3D PCASL) sequence. CBF maps from 3D PCASL images were coregistered between two MRI studies and with T2-weighted fluid-attenuated inversion recovery (3D FLAIR) images. Conventional magnetic resonance angiography (MRA) was performed with 3D time-of-flight (3D TOF), and maximum intensity projection (MIP) views were obtained.

Case report

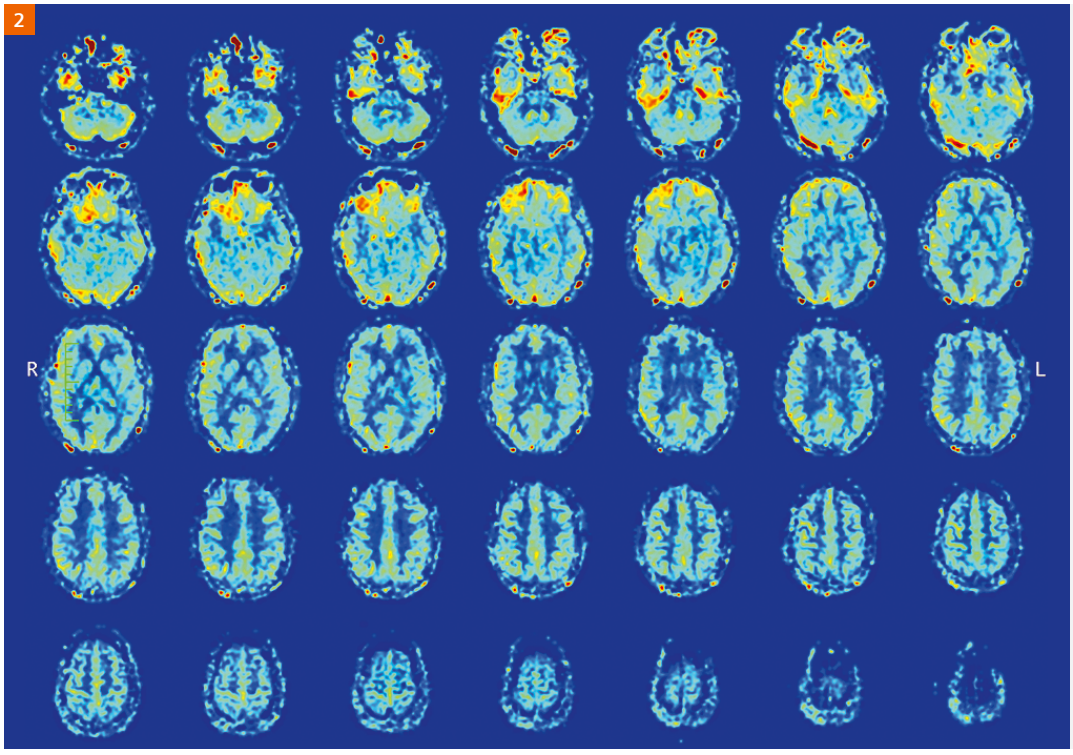

Figure 2: rCBF map (mL / 100 g / min) of a 31-year-old woman, acquired in the chronic phase using 3D PCASL five months from stroke onset when the basilar artery appeared normalized. The color map "jet" (blue/green: low perfusion, yellow/red: high perfusion) was used to map the image values.

In September 2017, a 31-year-old woman presented with a sudden severe headache, confusion, and amnesia that had developed after physical exertion. Conventional MRA showed an acute posterior circulation stroke involving the hippocampal formation and the anterior thalamus on the right side in particular. It also showed a stenosis of the distal basilar artery consistent with vasospasm. The patient was treated with nimodipine, which stopped the headache and rapidly improved her cognitive performance. Basilar artery lumen slowly normalized in the subsequent month.

Both during the subacute phase and five months later, besides MRA, we also assessed tissue lesions and brain perfusion with, respectively, 3D FLAIR and 3D PCASL sequences on a 3T MR scanner (MAGNETOM Skyra, Siemens Healthcare, Erlangen, Germany) equipped with a 20-channel head-neck coil. MRA images were obtained from 3D time-of-flight (3D TOF) images using the maximum intensity projection (MIP) in the Siemens Healthcare *syngo* software. The 3D FLAIR sequence was set up with the following parameters: Repetition/echo time (TR/TE): 5000/387 ms; inversion time (TI): 1800; slice thickness: 1 mm; matrix: 384 x 384; field of view (FOV): 229 x 229 mm2. The 3D PCASL sequence employs the 3D GRASE readout module and uses a pseudo-continuous labeling scheme with optional background suppression as described in [4–6]. It was set up with the following parameters: TR/TE: 4600/15.6 ms; FOV: 192 x 192 mm^2; slice thickness: 3 mm; labeling duration: 1500 ms; post-labeling delay: 1500 ms; M0 prescan. Total scan time including M0 was 5:27 min:sec (1 M0 image, 6 control/label image pairs). A rCBF map was also calculated from the prescan M0 and the label-control series using the formula in [3] and provided by the inline scanner software. 3D T1-weighted MPRAGE images were acquired as anatomical references to improve coregistration between series and exams (time points). The 3D T1 MPRAGE sequence used the following parameters: TR/TE: 5000/387 ms; TI: 1800; slice thickness: 1 mm; matrix: 256 x 256; FOV: 256 x 256 mm^2.

To facilitate a visual comparison of the results across the two time points, FLAIR and PCASL images were first registered to their corresponding MPRAGE images (acquired at the same time point) and then jointly registered to the common anterior-posterior commissure (ACPC) plane, as determined on the MPRAGE images, using affine transformations. Thereby, the FLAIR images and CBF maps from the two time points could be displayed using exactly the same transversal slice, which was selected on the FLAIR images to bisect a bilateral thalamic lesion that appeared as two hyperintense spots. The rCBF maps were obtained from perfusion-weighted maps using the M0 prescan and parameters in [7]. In addition, for display purposes, the same maps were also normalized to the maximum rCBF value (map peak).

Figures 1 and 2 show the rCBF maps provided from the inline scanner software from the 3D PCASL series acquired respectively in the subacute phase and after five months. The color maps were identically scaled using the same window.

Figure 3 shows the MRA and the 3D FLAIR/PCASL results after postprocessing (coregistration to the common ACPC plane, calculation of the rCBF values, and normalization to the maximum). For the MRA study, the coronal MIP views from the 3D TOF data show the stenosis of the distal basilar artery in the subacute phase (3A) and its normali-zation after five months (3E). The 3D FLAIR images and CBF maps are also shown in the subacute phase (3B, C) and after five months (3F, G). The FLAIR images show a bilateral thalamic lesion as two symmetrical hyperintense spots, which remained substantially unchanged between the subacute (3B) and chronic (3F) phases. The rCBF map in the subacute phase (3C) shows a serpiginous, high absolute CBF surrounding the lesion in the right thalamus, but not in the left. The CBF map normalized to the maximum rCBF value (3D) emphasizes this effect and further highlights inhomogeneous perfusion throughout the gray matter, with relatively low perfusion in the posterior circulation territories and in the right hemisphere. After five months, the rCBF map (3G) shows globally reduced levels of perfusion. However, the normalized CBF map (3H) in particular shows a more homogeneous perfusion pattern throughout the gray matter.

This case illustrates how 3D PCASL CBF measurements can potentially add value beyond the conventional MRA findings. In fact, although MRA allows (in this case) to locate the stenosis, the CBF map provides a richer pattern of the stroke effects, even beyond the territory supplied by the narrowed artery. Specifically, the CBF map in the subacute phase seems to indicate the possible presence (and the distant metabolic consequences) of collateral circulation induced by the hemodynamic adaptation to the stroke event. In fact, when the arterial arrival time exceeds the post-labeling delay (the time required for spins to travel from the labeling plane to the imaged slice), labeled spins become visible as bright intra-arterial high signals. This effect is known as "arterial transit artefact" (ATA) [8] to emphasize that the signal comes not from the parenchyma but from the vessel (an unwanted effect under physiological conditions). Such intravascular signals can be attributed to the

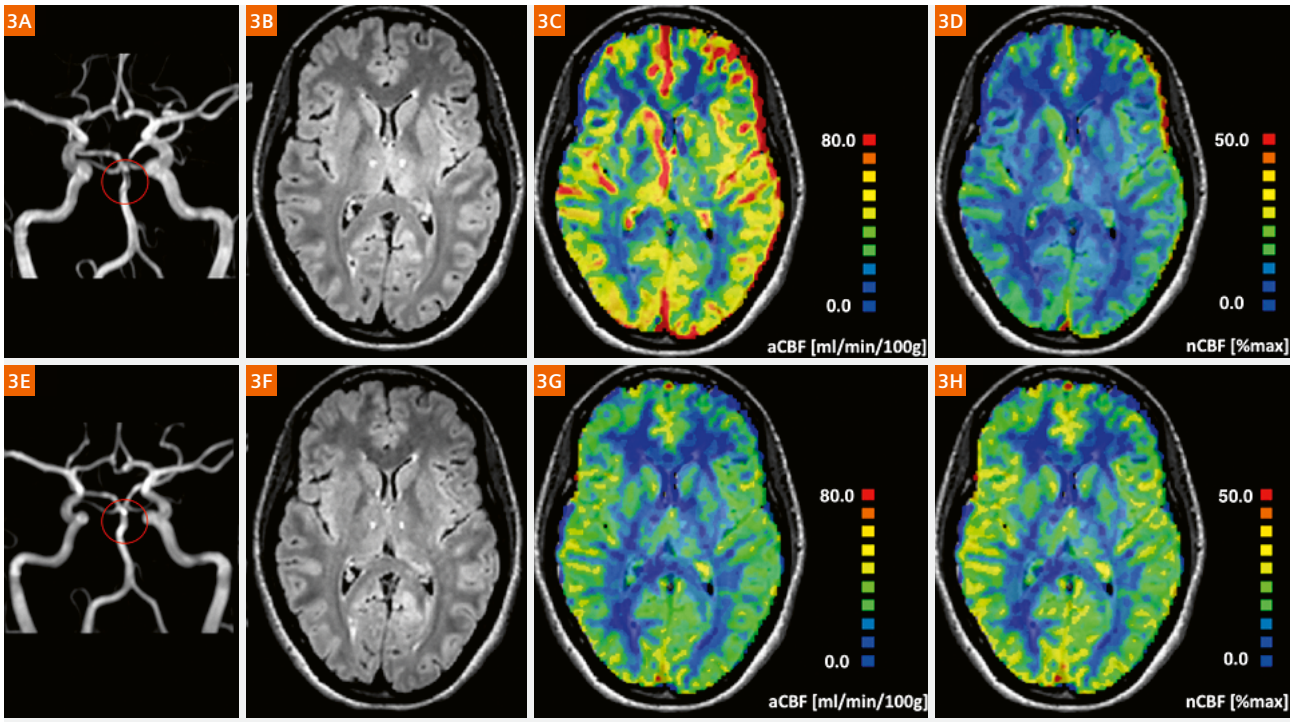

Figure 3:
MRA-FLAIR-ASL study re-elaboration (coregistration to common ACPC plane, CBF normalization): **(3A)** A 31-year-old woman with a stenosis of the distal basilar artery on MRA (coronal MIP from 3D TOF images); **(3B)** the FLAIR image in the subacute phase shows bilateral thalamic lesions; **(3C)** 3D PCASL shows a serpiginous, high absolute CBF close to the lesion in the right thalamus, but not in the left; **(3D)** normalized CBF shows inhomogeneous perfusion throughout the gray matter, and relatively low perfusion in the posterior circulation territories and the right hemisphere; **(3E)** after five months, the basilar artery has normalized on MRA (coronal MIP from 3D TOF images); **(3F)** the thalamic lesions did not change substantially on the FLAIR image; **(3G)** absolute CBF from 3D PCASL images shows globally reduced perfusion; **(3H)** normalized CBF shows more homogeneous perfusion throughout the gray matter.

slow-flowing (stagnant) blood upstream of the occlusion site, and it has repeatedly been shown [9] that detecting stagnant flow using a PCASL sequence can fruitfully complement MRA in localizing occlusions in acute stroke. This notion was substantially supported by our case, where the ATA disappeared during the chronic phase once the artery lumen was normalized. In previous studies, the presence of ATA has also been correlated with an improved outcome (lack of progression to infarct and better clinical outcome) after acute stroke [10]. It could, therefore, indicate the presence of compensating collat-eral flow, which would be a useful prognostic marker. Alternatively, regional increases in CBF values might indicate a "luxury perfusion", which is a maximal arteriolar vasodilation caused by loss of autoregulatory mechanisms in the tissue damaged by recent ischemia [11]. Luxury perfusion is also associated with an improved outcome for the ischemic penumbra.
Of particular interest is the detection of CBF changes in regions far beyond the territory supplied by the affected artery. In this case, CBF probably indicates functional phenomena due to the involvement of strategic brain regions (such as the thalami and the hippocampal formations) that might result in cerebral diaschisis with metabolic suppression far away from
the ischemic territory.

Overall, 3D PCASL can provide significant information that cannot be easily produced with other noninvasive techniques, and might provide new insight into the functional, vascular, and neuronal changes that often coexist with an ischemic brain accident.

These techniques, when used in a routine clinical setting, will make it possible to noninvasively and rapidly collate quantitative parameters that could be useful predictors of outcome and provide a more in-depth understanding of metabolic and vascular phenomena caused by a cerebro-afferent vessel occlusion. Ultimately, this could improve tailored approaches to treating ischemic stroke.

References

1 Haller S, Zaharchuk G, Thomas DL, Lovblad K-O, Barkhof F, Golay X. Arterial Spin Labeling Perfusion of the Brain: Emerging Clinical Applications. Radiology. 2016;281(2):337–56.

2 Harston GWJ, Okell TW, Sheerin F, Schulz U, Mathieson P, Reckless I, et al. Quantification of serial cerebral blood flow in acute stroke using arterial spin labeling. Stroke. 2017;48(1):123–30.
3 Alsop DC, Detre JA, Golay X, Günther M, Hendrikse J, Hernandez-Garcia L, et al. Recommended implementation of arterial spin-labeled Perfusion mri for clinical applications: A consensus of the ISMRM Perfusion Study group and the European consortium for ASL in dementia. Magn Reson Med. 2015;73(1):102–16.
4 Dai W, Garcia D, De Bazelaire C, Alsop DC. Continuous flow-driven inversion for arterial spin labeling using pulsed radio frequency and gradient fields. Magn Reson Med. 2008;60(6):1488–97.
5 Dai W, Robson PM, Shankaranarayanan A, Alsop DC. Reduced resolution transit delay prescan for quantitative continuous arterial spin labeling perfusion imaging. Magn Reson Med. 2012;67(5):1252–65.
6 Wu W-C, Fernández-Seara M, Detre JA, Wehrli FW, Wang J. A theoretical and experimental investigation of the tagging efficiency of pseudocontinuous arterial spin labeling. Magn Reson Med. 2007 Nov;58(5):1020–7.
7 Wang J, Zhang Y, Wolf RL, Roc AC, Alsop DC, Detre JA. Amplitude-modulated Continuous Arterial Spin-labeling 3.0-T Perfusion MR Imaging with a Single Coil: Feasibility Study. Radiology. 2005 Apr;235(1):218–28.
8 Detre JA, Samuels OB, Alsop DC, Gonzalez-At JB, Kasner SE, Raps EC. Noninvasive magnetic resonance imaging evaluation of cerebral blood flow with acetazolamide challenge in patients with cerebrovascular stenosis. J Magn Reson Imaging. 1999 Nov;10(5):870–5.
9 Sogabe S, Satomi J, Tada Y, Kanematsu Y, Kuwayama K, Yagi K, et al. Intra-arterial high signals on arterial spin labeling perfusion images predict the occluded internal carotid artery segment. Neuroradiology. 2017 Jun 10;59(6):587–95.
10 Chng SM, Petersen ET, Zimine I, Sitoh Y-Y, Lim CCT, Golay X. Territorial Arterial Spin Labeling in the Assessment of Collateral Circulation: Comparison With Digital Subtraction Angiography. Stroke. 2008;39(12):3248–54.
11 Viallon M, Altrichter S, Pereira VM, Nguyen D, Sekoranja L, Federspiel A, et al. Combined Use of Pulsed Arterial Spin-Labeling and Susceptibility-Weighted Imaging in Stroke at 3T. Eur Neurol. 2010;64(5):286–96.

Contact

Fabrizio Esposito, Ph.D.
Department of Medicine, Surgery & Dentistry
Scuola Medica Salernitana
University of Salerno
Via S. Allende
84081 Baronissi
Italy
Tel.: +39 089 96 50 82
Fax: +39 089 96 88 43
faesposito@unisa.it

Ultrafast Brain Imaging with Deep Learning Multi-Shot EPI: Preliminary Clinical Evaluation

Azadeh Tabari[1], Bryan Clifford[2], Augusto Lio M. Goncalves Filho[1], Zahra Hosseini[3], Thorsten Feiweier[4], Wei-Ching Lo[2], Min Lang[1], Maria Gabriela Figueiro Longo[1], Kawin Setsompop[5], Berkin Bilgic[6], Otto Rapalino[1], Pamela Schaefer[1], Stephen Cauley[6], Susie Huang[1], John Conklin[1]

[1]Department of Radiology, Massachusetts General Hospital, Boston, MA, USA
[2]Siemens Medical Solutions USA, Boston, MA, USA
[3]Siemens Medical Solutions USA, Atlanta, GA, USA
[4]Siemens Healthineers, Erlangen, Germany
[5]Department of Radiology / Department of Electrical Engineering, Stanford University, Stanford, CA, USA
[6]Department of Radiology, A. A. Martinos Center for Biomedical Imaging, Massachusetts General Hospital, Harvard Medical School, Boston, MA, USA

MR imaging (MRI) is an integral part of the diagnosis and treatment planning of various neurological diseases. However, the long scan time of brain MRI is a major factor that limits its effectiveness, especially in patients who are prone to motion and frequently require sedation. Thus, fast brain MRI protocols with acceptable diagnostic image quality are desired to enable wider clinical application of MRI [1, 2]. There is an ongoing clinical need to reduce the scan time of brain MRI, especially for uncooperative or motion-prone patients, and patients with diseases requiring rapid diagnosis such as stroke.

Various efforts have been made to achieve ultrafast MRI for brain imaging by using pulse sequences that rapily acquire images. One well-known approach is to use

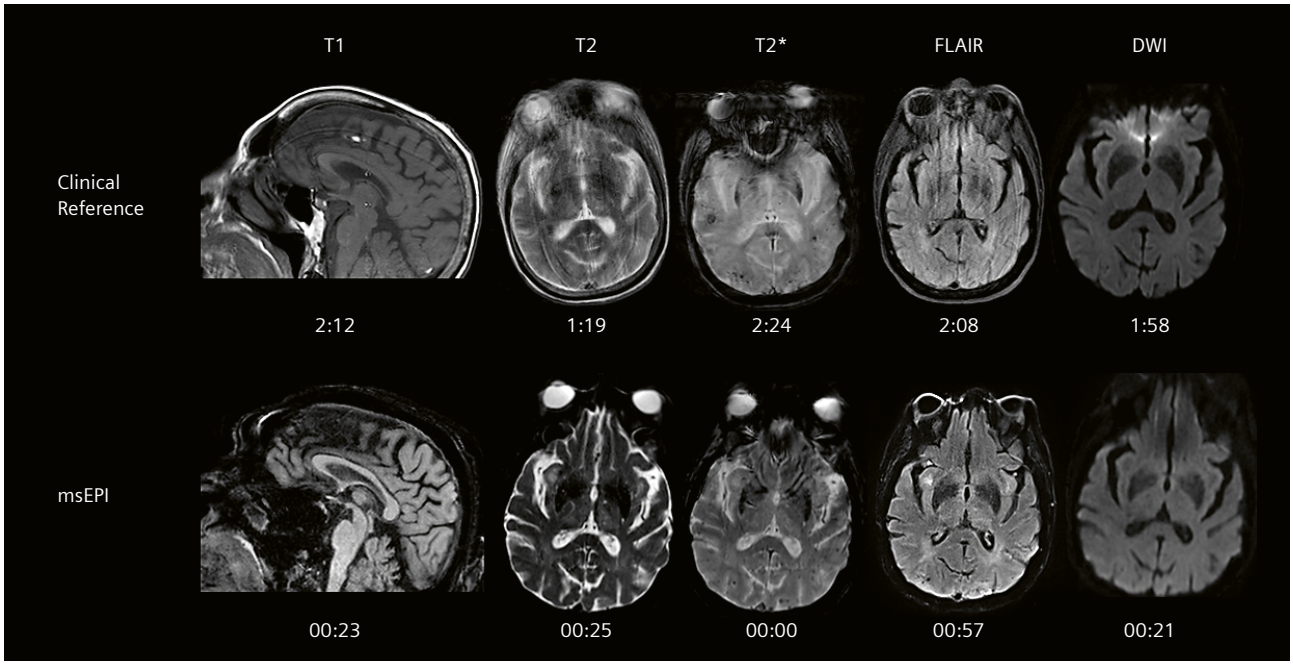

1 Illustrative example on the comparison of the motion-degraded exam of a 10-minute clinical reference protocol to the proposed 2-minute msEPI protocol in a 73-year-old female with no pathologic findings.

single-shot echo-planar imaging (ssEPI), which acquires *k*-space data for an entire 2D image in a single, long readout (shot), following a single RF-excitation pulse [3, 4]. The number of *k*-space lines (echoes) collected in a single shot is called the "EPI factor". The technical advances in the design of echo-planar imaging have made ultrafast brain MRI protocols, including a combination of anatomic and functional sequences, possible [5, 6]. ssEPI methods have recently been used to create rapid screening exams with total durations of 1–2 minutes. However, these rapid ssEPI approaches come at the cost of significant geometric distortion, low signal-to-noise ratio (SNR), and reduced tissue contrast [6–8]. In addition, these approaches offer limited flexibility to acquire in different image orientations or to repeat individual contrasts.

Multi-shot EPI (msEPI) acquisitions have been exploited to address these shortcomings. In a msEPI acquisition, data from multiple highly-undersampled shots are combined together. This approach results in reduced geometric distortion, but at the cost of slightly longer scan times. Higher acceleration factors can be used to compensate for this, but can lead to increased *g*-factor noise and residual aliasing [9–11]. Recent advancement in artificial intelligence (AI)-powered reconstruction algorithms have proved successful in denoising accelerated MRI data. Deep learning (DL) models, can be applied to reduce noise and residual aliasing during reconstruction [12].

In this article we show preliminary results from a clinical translational study being performed at Massachusetts General Hospital (MGH) for validating the feasibility of prototype DL-accelerated msEPI-based rapid brain protocols[1] in a high-volume emergency and inpatient care setting. The rapid imaging technique combines a novel deep learning algorithm to limit *g*-factor noise amplification, magnetization transfer preparation to improve brain tissue contrast, and high per-shot EPI undersampling factors to minimize geometric distortion [12, 13]. A multidisciplinary team of neuroradiologists, MR physicists, and Siemens Healthineers engineers at MGH have developed and optimized acquisition parameters for each of these prototype msEPI-based MRI protocols. Following the optimization of sequence parameters and DL-based reconstruction, an Institutional Review Board approved study was executed. The validation approach comprised prospective comparative studies of emergency and inpatient examinations with a variety of indications. The imaging protocol included T1-, T2-, T2*-weighted, T2-FLAIR, and DW imaging sequences from the prototype msEPI protocol and the clinical reference standard. Imaging was performed on 3T MRI scanners (MAGNETOM Skyra and MAGNETOM Prisma, Siemens Healthcare, Erlangen, Germany) using a 20-channel head coil. Fully sampled msEPI training data were acquired with two averages and eight shots across 16 healthy subjects (8 men, 8 women, aged 19–67). A single FLASH auto calibration scan, acquired at the start of each acquisition, allowed for the calculation of coil sensitivity maps, GRAPPA and/or SMS kernels. The data were split into training and validation datasets with 12 and 4 subjects, respectively. The use of fully sampled data allowed networks to be trained for different acceleration factors through retrospective undersampling.

Two board-certified neuroradiologists, blinded to the clinical history and the imaging protocols, evaluated the head-to-head image quality, scan time, and diagnostic performance of DL-accelerated msEPI-based MRI protocols against the respective clinical standard protocols. For diagnostic performance, they assessed six clinically relevant imaging findings in each protocol (intracranial mass-like lesion, intracranial hemorrhage, white matter hyperintensities, subarachnoid FLAIR hyperintensities, diffusion restriction, and hydrocephalus). For image quality, the raters used a 3-point score to evaluate image degradation by noise and artifacts. Qualitative assessment was compared using Wilcoxon signed-rank tests, and the intraclass correlation coefficients (ICCs) were used to test interobserver reproducibility on the diagnostic concordance between two readers.

Initial clinical experience

The prototype msEPI protocols (T1-, T2-, T2*-weighted, T2-FLAIR, and DWI) required only 2 minutes of scan time (not including adjustments), while the rapid reference protocols (turbo spin-echo (TSE)-based acquisitions) took 10 minutes for the same number of image contrasts. A total of 26 patients (Male:Female 12:14, mean age 58 ± 19 years old) were included in this preliminary study.

Two board-certified neuroradiologists performed an initial clinical subjective evaluation of the DL-accelerated msEPI-based images. Aside from noticeable mild distortion of soft facial tissues, the msEPI images contained only very minimal distortion of the pons and temporal lobes – areas which are critical for diagnosis. The limited artifacts we observed were most prevalent in the longer echo-time T2* data and corresponded to cases where patient motion could be identified. Figure 1 illustrates how shorter scan time allows for lower motion artifacts.

Interobserver agreement was 'almost perfect' for the evaluation of intracranial masses (ICC = 1), WM hyperintensities (ICC = 0.83), diffusion restrictions (ICC = 0.83), and hydrocephalus (ICC = 1); and 'substantial' for intracranial hemorrhage (ICC = 0.76) and subarachnoid FLAIR

[1] *Work in progress. The application is currently under development and is not for sale in the U.S. and in other countries. Its future availability cannot be ensured.*

hyperintensities (ICC = 0.65). Head-to-head comparisons of image quality showed increased noise on the msEPI exams for T1, FLAIR, and DWI ($p < 0.05$) and increased artifacts on T2, T2*, and FLAIR ($p < 0.05$), without compromising the detection of the imaging findings.

Figures 2–6 demonstrate examples of the msEPI images and the corresponding clinical reference images for each image contrast, highlighting the clinical findings in each. As these cases illustrate, the 2-minute DL-accelerated msEPI prototype sequences can offer high clinical efficacy at a significantly shorter acquisition time.

Conclusion

We have successfully used a DL-accelerated 2-minute msEPI protocol to enable rapid, comprehensive brain MRI evaluation of emergency department and hospitalized patients. In this preliminary study we found high interobserver agreement for major brain MRI findings, similar to that of a 10-minute conventional protocol. The DL-accelerated 2-minute msEPI protocol provided clear depiction of pathologic intracranial findings and comparable tissue contrast to that observed with the five-fold slower clinical reference exam. The msEPI technique is currently being evaluated in a larger clinical study of inpatient and emergency department patients at our institution, which

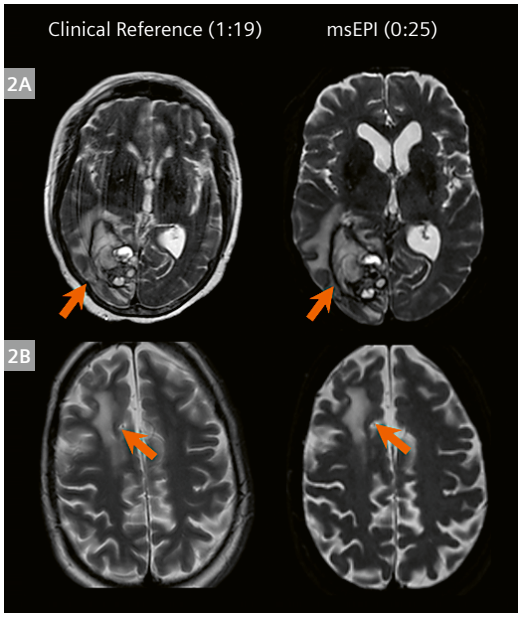

T2 Sequence	Acquisition Time (m:s)	Resolution (mm^3)	TR (ms)	TE (ms)	PAT Factor	No. shots	Echo spacing (ms)
TSE	1:19	0.9×0.9×5.0	7060	85	2	–	9.42
msEPI	0:25	1.0×1.0×4.0	4500	86	2	4	1.2

2 **(2A)** Large complex hemorrhagic mass-like lesion within the right occipital lobe that is better seen on msEPI exam. The clinical reference exam that was performed with > 3-fold increase in scan time demonstrates intense motion artifacts.
(2B) Post-surgical changes from right frontal craniotomy with right frontal lobe encephalomalacia.

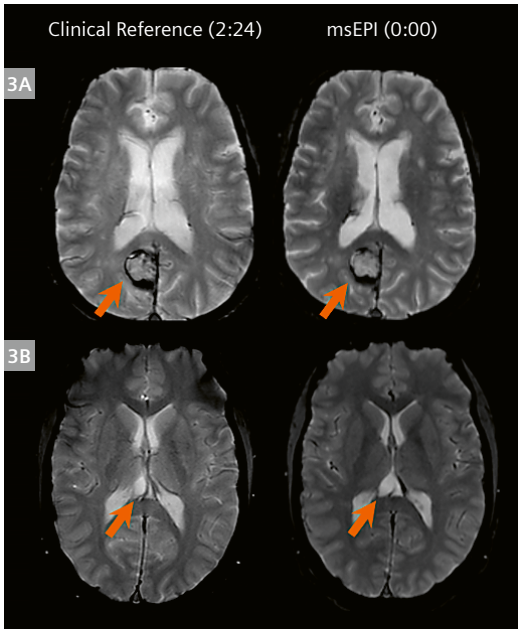

T2* Sequence	Acquisition Time (m:s)	Resolution (mm^3)	TR (ms)	TE (ms)	PAT Factor	No. shots	Echo spacing (ms)
GRE	2:24	0.9×0.9×5.0	694	20	1	–	–
msEPI	0:00[2]	1.0×1.0×4.0	4500	21.2	2	4	1.2

3 **(3A)** Right parietal lobe intraparenchymal hematoma with dependent T2* hypointense blood products.
(3B) Non-enhancing cystic lesion in the right aspect of the pineal gland.

[2] *Acquired in combination with the T2 sequence.*

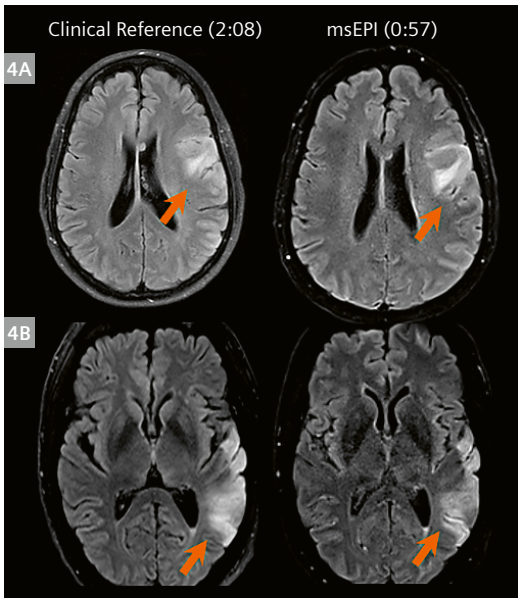

FLAIR Sequence	Acquisition Time (m:s)	Resolution (mm³)	TR (ms)	TE (ms)	PAT Factor	No. shots	Echo spacing (ms)
TSE	2:08	0.9×0.9×5.0	9000	85	2	–	7.49
msEPI	0:57	1.0×1.0×4.0	9000	86	2	2	1.19

4 **(4A)** Left frontal high-grade glioma.
(4B) Subacute left temporal lobe infarct (left middle cerebral artery territory).

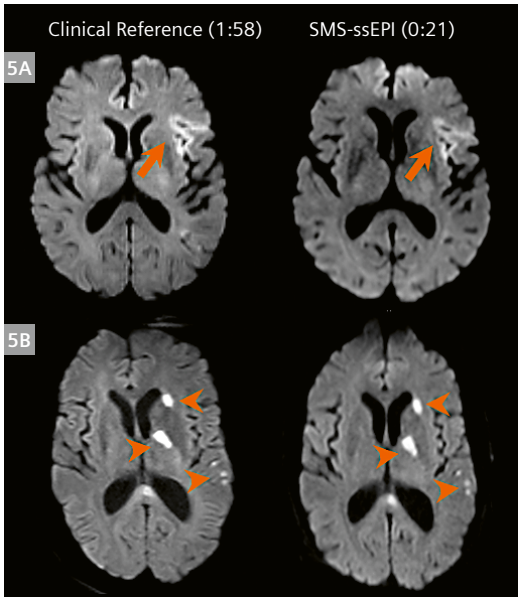

DWI Sequence	Acquisition Time (m:s)	Resolution (mm³)	TR (ms)	TE (ms)	PAT Factor	No. shots	Echo spacing (ms)
ssEPI	1:58	1.4×1.4×5.0	3800	72	2	1	0.72
SMS-ssEPI	0:21	1.4×1.4×4.0	2000	63	2	2	0.93

b-value 1000 s/mm²

5 **(5A)** Subacute infarct involving left frontal lobe and insula.
(5B) Multiple infarcts involving left cerebral hemisphere.

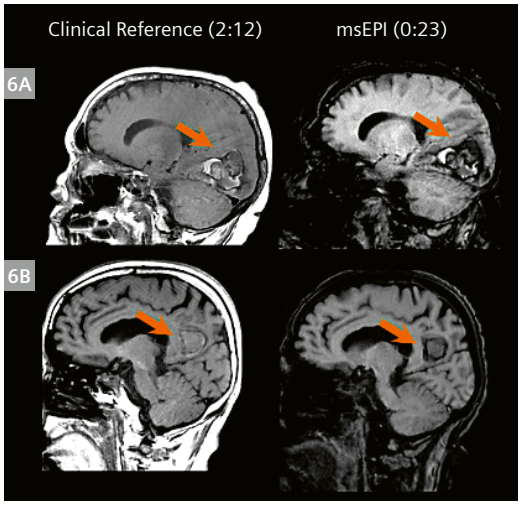

T1 Sequence	Acquisition Time (m:s)	Resolution (mm³)	TR (ms)	TE (ms)	PAT Factor	No. shots	Echo spacing (ms)
SE	2:12	0.9×0.9×4.0	400	8.4	1	–	–
msEPI	0:23	1.0×1.0×4.0	1670	12	2	4	1.18

6 **(6A)** Hemorrhagic neoplastic lesion in the right occipital lobe.
(6B) Right parietal lobe intraparenchymal hematoma.

will provide further insight into the advantages and trade-offs of ultrafast, high-quality brain imaging in this patient population. We envision this protocol could be an effective rapid screening tool for acute intracranial pathology in these often difficult to image and neurologically unstable patients.

References

1 Blystad I, Warntjes JB, Smedby O, et al. Synthetic MRI of the brain in a clinical setting. Acta Radiol 2012; 53:1158–1163

2 Raja, A. S. et al. Radiology Utilization in the Emergency Department: Trends of the Past 2 Decades. Am J Roentgenol. 203, 355–360 (2014).

3 Sun K, Zhong Z, Xu Z, et al. In-plane simultaneous multisegment imaging using a 2D RF pulse. Magn Reson Med. 2021 Aug 4. doi: 10.1002/mrm.28956. Epub ahead of print. PMID: 34350601.

4 Feinberg DA, Moeller S, Smith SM, et al. Multiplexed echo planar imaging for sub-second whole brain FMRI and fast diffusion imaging. PLoS One. 2010 Dec 20;5(12):e15710. doi: 10.1371/journal.pone.0015710. Erratum in: PLoS One. 2011;6(9).

5 Ha JY, Baek HJ, Ryu KH, et al. One-Minute Ultrafast Brain MRI With Full Basic Sequences: Can It Be a Promising Way Forward for Pediatric Neuroimaging? AJR Am J Roentgenol. 2020 Jul;215(1):198-205. doi: 10.2214/AJR.19.22378. Epub 2020 Apr 7. PMID: 32255685.

6 Setsompop K, Feinberg DA, Polimeni JR. Rapid brain MRI acquisition techniques at ultra-high fields. NMR Biomed. 2016 Sep;29(9):1198-221. doi: 10.1002/nbm.3478. Epub 2016 Feb 2. PMID: 26835884; PMCID: PMC5245168.

7 Skare S, Sprenger T, Norbeck O, et al. A 1-minute full brain MR exam using a multicontrast EPI sequence. Magn Reson Med. 2018;79(6):3045-3054. doi:10.1002/mrm.26974

8 Ryu KH, Choi DS, Baek HJ, et al. Clinical feasibility of 1-min ultrafast brain MRI compared with routine brain MRI using synthetic MRI: a single center pilot study. J Neurol. 2019;266(2):431-439. doi:10.1007/s00415-018-9149-4

9 Liao C, Bilgic B, Tian Q, et al. Distortion-free, high-isotropic-resolution diffusion MRI with gSlider BUDA-EPI and multicoil dynamic B 0 shimming. Magn Reson Med. March 2021:mrm.28748. doi:10.1002/mrm.28748

10 Chen N, Guidon A, Chang H-C, Song AW. A robust multi-shot scan strategy for high-resolution diffusion weighted MRI enabled by multiplexed sensitivity-encoding (MUSE). NeuroImage. 2013;72:41-47. doi:10.1016/j.neuroimage.2013.01.038

11 Conklin, J. et al. A comprehensive multi-shot EPI protocol for high-quality clinical brain imaging in 3 minutes. Proc. Intl. Soc. Magn. Reson. Med. 6691 (2020).

12 Clifford B, Conklin J, Huang S, et al. Clinical evaluation of an AI-accelerated two-minute multi-shot EPI protocol for comprehensive high-quality brain imaging. In: Proceedings of the 28th Annual Meeting of ISMRM, virtual, USA, 2020.

13 Demir S, Clifford B, Feiweier T, et al. Optimization of magnetization transfer contrast for EPI FLAIR brain imaging. International Society for Magnetic Resonance in Medicine, 2021. Online virtual meeting.

Contact

John Conklin, M.D., MS
Diagnostic Radiologist
Director of Emergency MRI
Division of Emergency Imaging
Department of Radiology
Massachusetts General Hospital
326 Cambridge St #410
Boston, MA 02114
USA
Phone: +1617-726-8323
John.Conklin@MGH.HARVARD.EDU

Ultrafast Brain Imaging with Deep-Learning Multi-Shot EPI: Technical Implementation

Bryan Clifford[1], John Conklin[2], Susie Y. Huang[2], Thorsten Feiweier[3], Zahra Hosseini[4], Azadeh Tabari[2], Augusto Lio M. Goncalves Filho[2], Serdest Demir[2], Wei-Ching Lo[1], Stephan Kannengiesser[3], Dominik Nickel[3], Min Lang[2], Maria Gabriela Figueiro Longo[2], Michael Lev[2], Pam Schaefer[2], Otto Rapalino[2], Kawin Setsompop[5], Berkin Bilgic[6], Stephen Cauley[6]

[1]Siemens Medical Solutions USA, Boston, MA, USA
[2]Department of Radiology, Massachusetts General Hospital, Boston, MA, USA
[3]Siemens Healthineers, Erlangen, Germany
[4]Siemens Medical Solutions USA, Atlanta, GA, USA
[5]Department of Radiology and Department of Electrical Engineering, Stanford University, Stanford, CA, USA
[6]Department of Radiology, A. A. Martinos Center for Biomedical Imaging, Massachusetts General Hospital, Harvard Medical School, Boston, MA, USA

This work was performed using a prototype that led to the development of the Deep Resolve Swift Brain product.

Introduction

MRI is a crucial tool for the diagnosis and treatment planning of neurological diseases. Compared to CT and ultrasound, however, the underlying physics of the MR imaging process necessitates relatively long acquisition times. This has limited the use of brain MRI in time- or motion-sensitive settings, such as the emergency department, where long or repeated scans can delay urgently needed treatment [1–4].

The integration of parallel imaging (PI) and simultaneous multi-slice (SMS) imaging techniques [5–8] into standard turbo-spin-echo (TSE)-based clinical protocols has allowed for exam times of approximately 10 minutes. Advances in 3D volumetric encoding schemes [9], compressed sensing [10], and deep-learning (DL) reconstruction techniques [11–13] have helped alleviate the geometry-factor (*g*-factor) noise amplification of standard PI and SMS techniques to provide additional acceleration and further reduce exam times. Current application of these techniques to standard TSE-based protocols has lead to exam times of approximately 5 minutes [14–16].

Recently, single-shot echo-planar imaging (ssEPI) has been used to enable ultrafast multi-contrast exams on the order of 1–2 minutes [17, 18]. ssEPI acquisitions acquire all *k*-space lines after a single excitation or "shot" and allow for very rapid scan times, but require longer readout durations and echo times. As such, ssEPI images often suffer from susceptibility-induced geometric distortion as well as signal dropout and pileup artifacts.

To take advantage of the efficiency of EPI while mitigating signal-to-noise (SNR) and susceptibility-induced losses to image quality, we have developed a multi-shot EPI (msEPI)-based prototype[1] that leverages a DL-based image reconstruction to provide high-SNR T1w, T2w, T2*, and T2-FLAIR, complemented by ssEPI diffusion imaging within a 2-minute exam. The prototype's msEPI acquisition acquires readout lines in an interleaved fashion across several shots to achieve shorter echo times and reduce geometric distortion. At the same time, the DL-based image reconstruction produces high-SNR images and limits *g*-factor noise amplification. To provide greater flexibility and robustness to variations in the clinical workflow, the prototype allows each contrast to be acquired individually, in any orientation, and the DL-reconstruction includes a tunable parameter which can be automatically selected to optimize image quality and data fidelity.

In the following sections, we describe the prototype's data acquisition and image reconstruction methods, and provide performance evaluation metrics and preliminary results on clinical data not included during training.

Data acquisition

Prototype sequences were developed for acquiring T1w, T2w, T2*, FLAIR, and diffusion-weighted imaging data. Multi-shot acquisitions with high per-shot undersampling factors were used for all but the DWI sequence, which was

[1]*Work in progress. The application is currently under development and is not for sale in the U.S. and in other countries. Its future availability cannot be ensured.*

acquired using an SMS ssEPI acquisition. T2w and T2* contrasts are obtained before and after the refocusing pulse of the same msEPI scan, which further increases the sampling efficiency. To provide robustness against intra-scan motion and allow for the individual acquisition of any contrast, each scan was preceded by a fast FLASH reference scan [19], which was used to compute coil sensitivity maps, GRAPPA [5], and/or SMS kernels [20]. Additional information on the data acquisition is provided in [21].

Clinical evaluation data were acquired on patients and healthy volunteers using a 20-channel head/neck coil and a 64-channel head coil on 3T systems (MAGNETOM Prisma and Vida, Siemens Healthcare, Erlangen, Germany) with informed written consent and in accordance with local IRB guidelines. Clinical reference data were acquired for comparison immediately before the prototype exam using a standard 10-minute clinical exam. Protocol parameters from both exams are shown in Figure 1.

A deep-learning network was trained using a dataset consisting of more than 26,000 images across T1w, T2w, T2*, and T2-FLAIR contrasts in axial, coronal, and sagittal orientations (Fig. 2). The 2-average data for network training and validation were acquired on a 3T system (MAGNETOM Skyra, Siemens Healthcare, Erlangen, Germany) using a 20-channel head/neck coil.

Deep-learning hybrid image reconstruction

The prototype sequences use a novel image reconstruction algorithm that integrates DL priors into an iterative SENSE [22] reconstruction (Fig. 3). Undersampled data acquired from the scanner are first passed through a standard

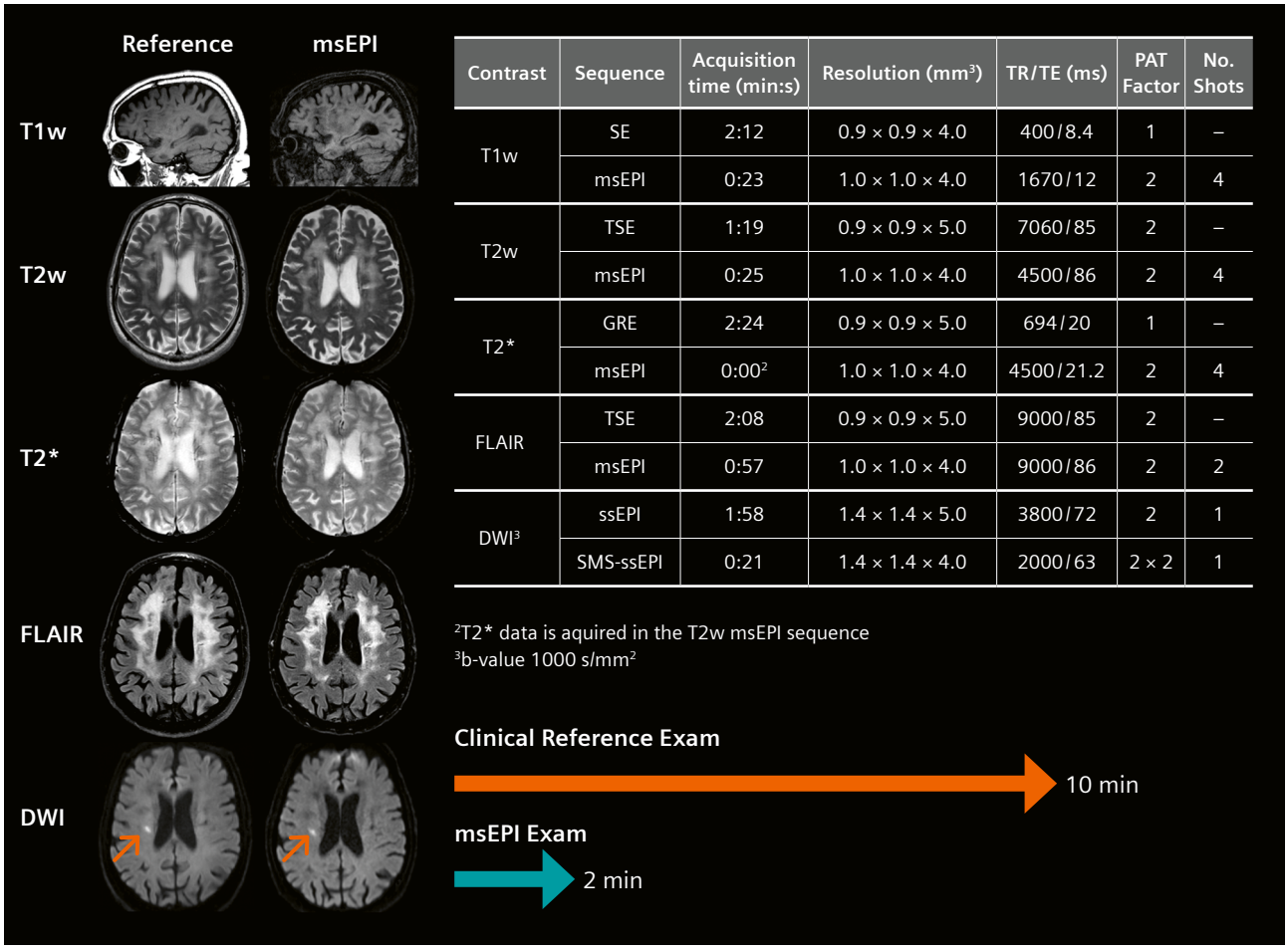

Contrast	Sequence	Acquisition time (min:s)	Resolution (mm³)	TR/TE (ms)	PAT Factor	No. Shots
T1w	SE	2:12	0.9 × 0.9 × 4.0	400/8.4	1	–
	msEPI	0:23	1.0 × 1.0 × 4.0	1670/12	2	4
T2w	TSE	1:19	0.9 × 0.9 × 5.0	7060/85	2	–
	msEPI	0:25	1.0 × 1.0 × 4.0	4500/86	2	4
T2*	GRE	2:24	0.9 × 0.9 × 5.0	694/20	1	–
	msEPI	0:00[2]	1.0 × 1.0 × 4.0	4500/21.2	2	4
FLAIR	TSE	2:08	0.9 × 0.9 × 5.0	9000/85	2	–
	msEPI	0:57	1.0 × 1.0 × 4.0	9000/86	2	2
DWI[3]	ssEPI	1:58	1.4 × 1.4 × 5.0	3800/72	2	1
	SMS-ssEPI	0:21	1.4 × 1.4 × 4.0	2000/63	2 × 2	1

[2]T2* data is aquired in the T2w msEPI sequence
[3]b-value 1000 s/mm²

1 Preliminary clinical results and protocol parameters of the msEPI and clinical reference exam. Images were obtained from a patient not included in the training or validation datasets, with a recent right corona radiata lacunar infarct (DWI images, arrows) and extensive white matter T2-FLAIR hyperintense signal abnormality likely related to cerebral small vessel disease. A graphical representation of the total acquisition times in the clinical reference and msEPI exams is included below the parameter table.

parallel imaging reconstruction, e.g., SENSE, which is used as input to an unrolled gradient-descent network (UGDN) [11]. The UGDN removes residual aliasing artifacts and noise from the initial reconstruction by iteratively passing the image through a deep neural network followed by a data-fidelity increasing operation which incorporates the physics of the acquisition and original measured data. The output of the UGDN, which will have good SNR but may be overly smooth, is then refined in a second iterative SENSE reconstruction, referred to as the DL-SENSE hybrid reconstruction [21].

The DL-SENSE hybrid reconstruction uses the image from the UGDN to regularize an iterative SENSE reconstruction and so generate a high-SNR image with good data fidelity and preservation of fine details. Specifically, the DL-SENSE hybrid reconstruction is a generalization of the methods in [23, 24] and computes the final image by solving the following optimization problem:

$$\min_{\boldsymbol{\rho}} || \boldsymbol{d} - \Omega \mathrm{FC}\boldsymbol{\rho} ||_2^2 + \lambda || \mathrm{WFC}(\boldsymbol{\rho}_{\mathrm{UGDN}} - \boldsymbol{\rho}) ||_2^2$$

where $\boldsymbol{d}$ and $\boldsymbol{\rho}$ are vectors of the measured data and image values, respectively; $\boldsymbol{\rho}_{\mathrm{UGDN}}$ is the output of the UGDN; F and C are the Fourier encoding and coil sensitivity operators; Ω is the *k*-space sampling operator; λ is a tunable denoising parameter; W is a diagonal weighting matrix.

A key feature of the DL-SENSE hybrid reconstruction is its ability to provide explicit control over the way the UGDN influences the final reconstructed image, which allows the same network to be applied to data acquired under novel noise conditions without the need for costly retraining. The user can control the balance between the fidelity of the final image with the measured data (left term in the above optimization problem) and with the output of the UGDN (right term in the above optimization problem) by tuning the denoising parameter λ. Similarly, the weighting matrix W controls the spectral mixing of information from the UGDN image and the measured data. In the current prototype, W was chosen as a sampling operator with the same undersampling factor as Ω but with complementary sample locations. For a given value of λ, this choice of W provided a desirable tradeoff between data fidelity and image quality and helped to focus the UGDN's representational power on unsampled *k*-space regions during training.

Network training and validation

The UGDNs used by the prototype were trained using images from a dataset consisting of more than 26,000 images across all contrasts and orientations (Fig. 2). During training, simulated training examples were generated by retrospectively undersampling high-SNR images, and noise was added to the simulated data to match clinical SNR levels. Separate UGDNs were trained for undersampling (PAT) factors of 2, 3, and 4. Networks were trained to minimize a loss function consisting of a weighted combination of the structural similarity index measure (SSIM) – known to correlate with radiologist quality rating [25, 26] – and the mean absolute error between the reconstructed images and their corresponding ground-truths.

Approximately 6,500 images in the dataset were excluded from training and reserved for validation of the trained networks. Following the same procedure used during training, noisy, undersampled data were generated from these images and reconstructed using the DL-SENSE hybrid scheme. The mean ± SD of the SSIM values between the reconstructed images and their corresponding ground-truth images are shown in Figure 2, sorted by contrast and PAT factor. These results indicate that the proposed method can reliably generate high-quality images, even at higher (≥ 3) acceleration factors.

Automatic selection of the denoising parameter

It can be challenging to select an appropriate denoising parameter given the variability seen in clinical settings. For a given protocol, the denoising parameter can be manually tuned according to radiologist preference; however, the ideal choice can vary with changes to protocol parameters, coil loading, coil selection, etc., which are common in the clinic. The parameter that yields the best results in one scenario may lead to overly smooth or noisy images in another scenario.

This problem was addressed by training a model to automatically select the denoising parameter based on estimated data SNR. The prototype computes the noise level using acquisition-specific noise calibration data and combines this with an estimate of the signal intensity to compute the SNR. A trained model then uses the estimated SNR to predict the denoising parameter preferred by radiologists [27]. This automatic, data-driven adaptation of the denoising parameter makes the prototype robust to changes in protocol parameters and automatically reduces the impact of the DL prior on the reconstruction in higher SNR (or lower PAT factor) scenarios, to maximize data fidelity while preserving image quality.

Figure 4A shows both the GRAPPA and DL-SENSE hybrid reconstructions of T2-FLAIR data (the contrast with lowest SNR) acquired from a healthy volunteer at PAT 2, 3, and 4. The GRAPPA reconstructions show the expected noise amplification with increasing PAT factor, but in the DL-SENSE hybrid reconstruction, the noise levels remain

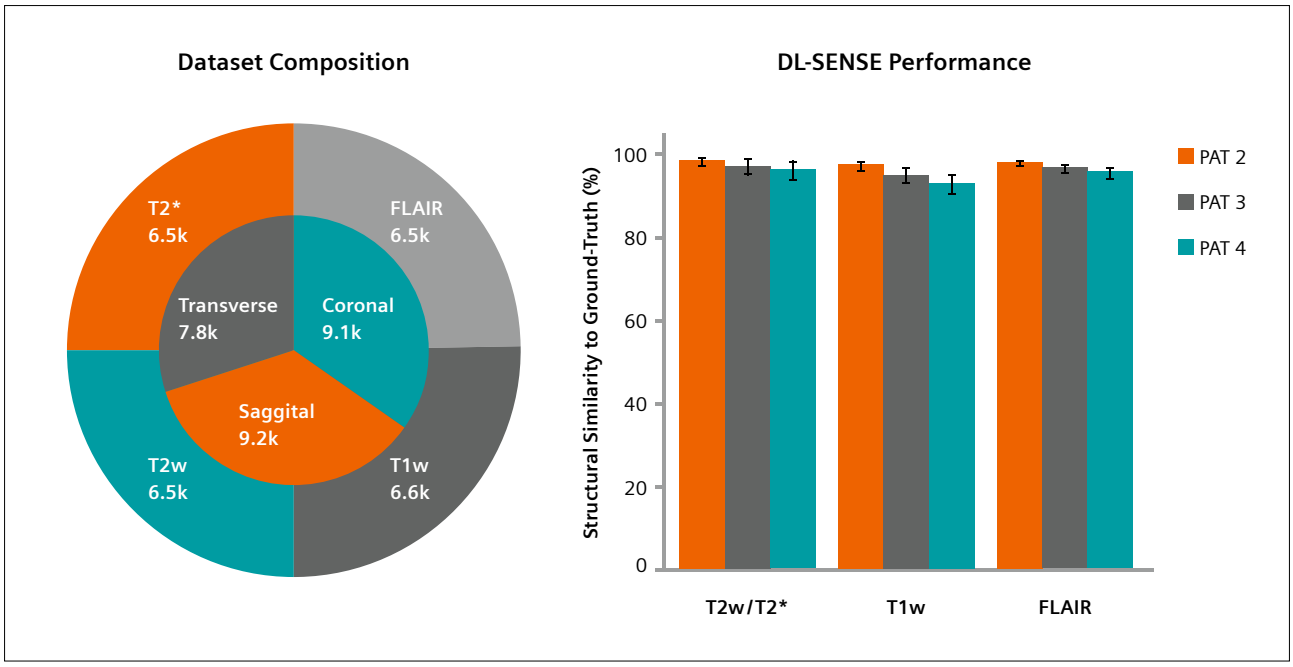

2 Dataset composition and validation results. The dataset consisted of more than 26,000 images and included T1w, T2w, T2*, and T2-FLAIR contrasts as well as coronal, sagittal, and transverse orientations, as shown in the pie chart. The bar chart shows the mean ± SD structural similarity index measure (SSIM) between DL reconstructions and the corresponding ground-truth validation images.

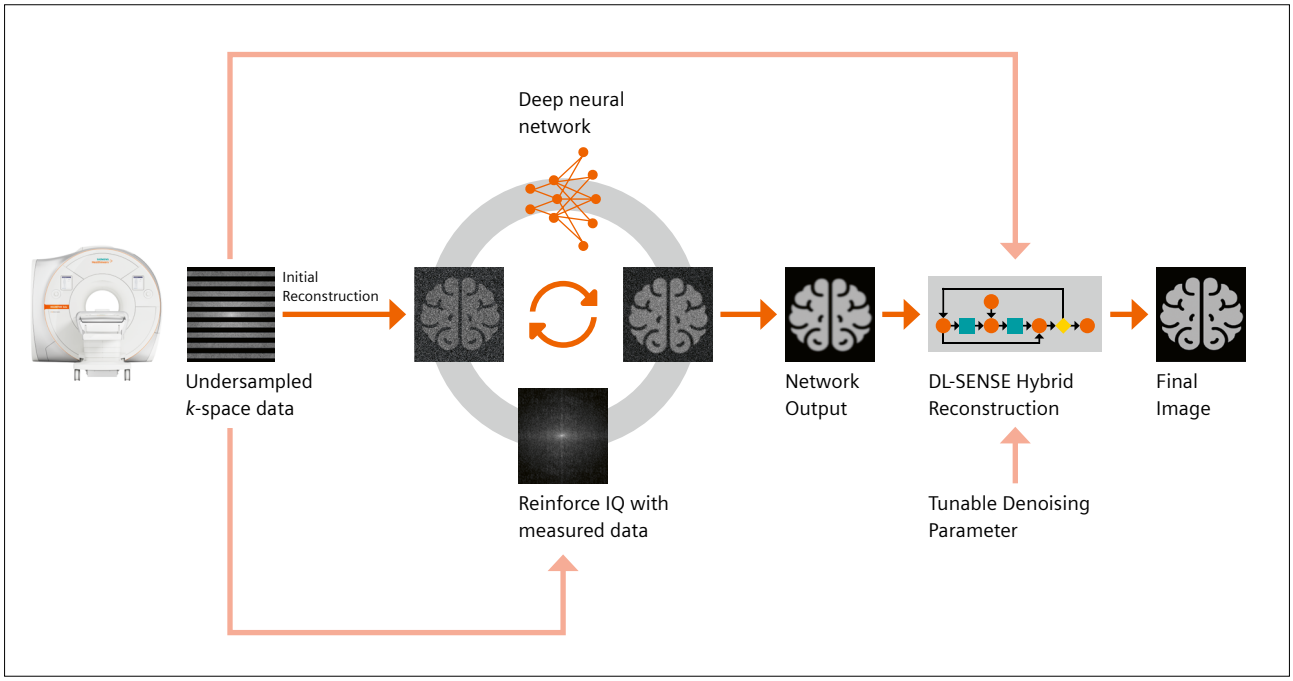

3 Illustration of the proposed reconstruction scheme. An initial SENSE reconstruction is generated from the undersampled *k*-space data and used as input to an unrolled gradient descent network (UGDN). The UGDN repeatedly alternates between deep neural-network denoising and data-fidelity updates to remove noise and residual aliasing while preserving the information in the acquired data. The UGDN output image and the measured data are then used in a regularized DL-SENSE hybrid reconstruction to produce the final image. By incorporating a tunable denoising parameter, the DL-SENSE hybrid reconstruction can be tailored to radiologist preference and also allows the same network to be applied to data acquired under noise conditions not previously seen without retraining.

relatively constant. Examination of representative denoising parameter values (orange markers in Figure 4B) shows that the trained model (orange line in Fig. 4B) automatically adjusts the denoising parameter as the PAT factor increases, using higher values for higher PAT factors. Figure 4B also shows example denoising parameter values from different contrasts and demonstrates how the model uses lower values for higher SNR contrasts (e.g., T2*) as well.

Reconstructions of T2-FLAIR data acquired on the same healthy volunteer using 20- and 64-channel coils are shown in Figure 5. Overall, the SNR of the two images is similar, but in the cortical region, the SNR of the 64-channel image is noticeably higher. These results suggest that the prototype can also adapt to changes in coil selection, allowing users to make the most out of higher density array coils.

Preliminary clinical results

We compared the proposed 2-minute prototype protocol to a standard TSE-based, 10-minute clinical reference protocol on a patient suffering from a recent right corona radiata lacunar infarct (DWI with restricted diffusion, Fig. 1 arrowheads) and extensive patchy and confluent

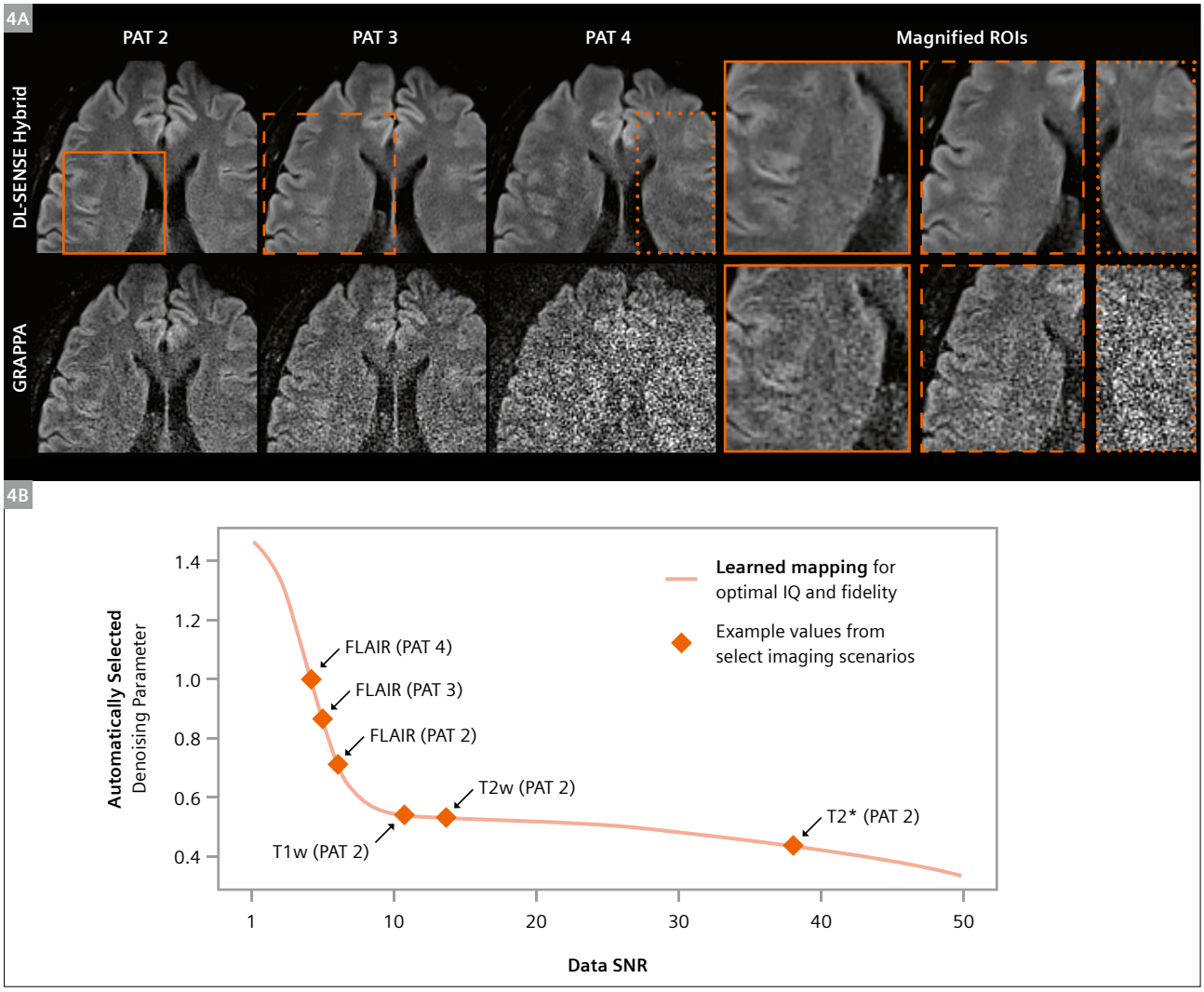

4 Generalization of the DL-SENSE hybrid reconstruction to higher undersampling (PAT) factors and varying SNR levels. **(4A)** Reconstructions of T2-FLAIR data acquired from a healthy volunteer at different PAT factors using the DL-SENSE hybrid reconstruction and GRAPPA. Magnified ROIs displayed on the right show how the proposed DL-SENSE reconstruction automatically adapts the denoising parameter to maintain image quality despite variations in the undersampling factor. **(4B)** The learned mapping between data SNR and optimal denoising parameter (orange line). The mapping was trained to predict parameters chosen by board-certified radiologists. The parameter values for the T2-FLAIR reconstructions in (4A) as well as for representative T1w, T2w, and T2* acquisitions are depicted by orange markers. The trained model tries to provide an optimal balance between image quality and data fidelity; in high-SNR scenarios, the model chooses lower values to maintain image quality while increasing data fidelity.

T2-FLAIR hyperintense white matter signal abnormality likely related to cerebral small vessel disease (T2-FLAIR, Fig. 1). Evaluation of the Figure 1 images by board-certified neuroradiologists indicated that, despite the nearly 5-fold reduction in exam time, the diagnostic quality of the images produced by the prototype was similar to that of the standard 10-minute exam. The white matter signal abnormality as well as the DWI/FLAIR mismatch (indicating a recent infarct) in the infarcted region can be clearly observed in the T2w, T2*, FLAIR, and DWI images from each protocol. Moreover, the gray/white differentiation of the msEPI T1w acquisition is similar to that of the reference SE T1w scan, despite the differences in the respective contrast mechanisms.

Although msEPI T1w images do not optimally depict facial soft tissues, which can be useful in certain diagnostic situations, it is interesting to note that the msEPI T1w images appear to depict the white matter lesions with greater conspicuity than the reference SE acquisition (possibly due to the increased T2* weighting). Regardless, future development will include the evaluation of a GRE-based T1w prototype sequence for the purposes of providing a nearly distortion-free reference, suitable for observing facial soft tissues.

In addition to the results presented here, clinical evaluations of earlier versions of this prototype have also been performed, with similar results [21, 28]. In particular, the report by Tabari et al. [28] provides initial results from a clinical evaluation on a large cohort of inpatients and emergency department patients, which indicate a high degree of interobserver agreement for major diagnostic findings, similar to that of the 5-fold slower clinical reference exam.

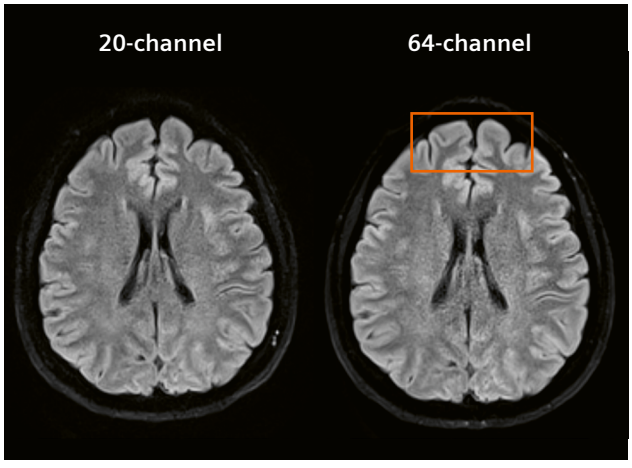

5 T2-FLAIR images acquired at 3T with the msEPI prototype sequence using the 20-channel head/neck coil and the 64-channel head coil from Siemens Healthineers. The msEPI prototype automatically adjusts the denoising level according to the SNR in each acquisition scenario, which makes it robust to variations in coil selection. To take advantage of the increased cortical sensitivity of the 64-channel coil, the prototype automatically reduces the denoising parameter in the DL-SENSE hybrid reconstruction to maximize IQ and data fidelity (see highlighted ROI).

Conclusions

We have developed an ultrafast MRI prototype that integrates a highly efficient msEPI acquisition with DL-based image reconstruction techniques to provide comprehensive brain MR imaging in a 2-minute exam. Although clinical evaluation on large patient cohorts is still ongoing, preliminary results indicate that the prototype can automatically adapt its DL reconstruction to variations in protocol parameters and coil selection to produce T1w, T2w, T2*, T2-FLAIR, and diffusion-weighted imaging with diagnostic quality similar to that of a standard 10-minute TSE-based acquisition.

References

1 Agarwal R, Bergey M, Sonnad S, Butowsky H, Bhargavan M, Bleshman MH. Inpatient CT and MRI utilization: trends in the academic hospital setting. J Am Coll Radiol. 2010;7(12):949–955.
2 Selvarajan SK, Levin DC, Parker L. The Increasing Use of Emergency Department Imaging in the United States: Is It Appropriate? AJR Am J Roentgenol. 2019;213(4):W180–W184.
3 Goyal M, Menon BK, van Zwam WH, Dippel DW, Mitchell PJ, Demchuk AM, et al. Endovascular thrombectomy after large-vessel ischaemic stroke: a meta-analysis of individual patient data from five randomised trials. Lancet. 2016;387(10029):1723–1731.
4 Berkhemer OA, Fransen PS, Beumer D, van den Berg LA, Lingsma HF, Yoo AJ, et al. A randomized trial of intraarterial treatment for acute ischemic stroke. N Engl J Med. 2015;372(1):11–20.
5 Griswold MA, Jakob PM, Heidemann RM, Nittka M, Jellus V, Wang J, et al. Generalized autocalibrating partially parallel acquisitions (GRAPPA). Magn Reson Med. 2002;47(6):1202–1210.
6 Pruessmann KP, Weiger M, Scheidegger MB, Boesiger P. SENSE: Sensitivity encoding for fast MRI. Magn Reson Med. 1999;42(5):952–962.
7 Glover GH. Phase-offset multiplanar (POMP) volume imaging: A new technique. J Magn Reson Imaging. 1991;1(4):457–61.
8 Barth M, Breuer F, Koopmans PJ, Norris DG, Poser BA. Simultaneous multislice (SMS) imaging techniques. Magn Reson Med. 2016;75(1):63–81.
9 Bilgic B, Gagoski BA, Cauley SF, Fan AP, Polimeni JR, Grant PE, et al. Wave-CAIPI for highly accelerated 3D imaging. Magn Reson Med. 2015;73(6):2152–2162.
10 Liang D, Liu B, Wang J, Ying L. Accelerating SENSE using compressed sensing. Magn Reson Med. 2009;62(6):1574–84.
11 Hammernik K, Schlemper J, Qin C, Duan J, Summers RM, Rueckert D. Systematic evaluation of iterative deep neural networks for fast parallel MRI reconstruction with sensitivity-weighted coil combination. Magn Reson Med. 2021;86(4):1859–1872.
12 Schlemper J, Caballero J, Hajnal JV, Price AN, Rueckert D. A Deep Cascade of Convolutional Neural Networks for Dynamic MR Image Reconstruction. IEEE Trans Med Imaging. 2018;37(2):491–503.

13 Aggarwal HK, Mani MP, Jacob M. MoDL: Model Based Deep Learning Architecture for Inverse Problems. IEEE Trans Med Imag. 2019;38(2):394–405.
14 Prakkamakul S, Witzel T, Huang S, Boulter D, Borja MJ, Schaefer P, et al. Ultrafast Brain MRI: Clinical Deployment and Comparison to Conventional Brain MRI at 3T. J Neuroimaging. 2016;26(5):503–510.
15 Recht MP, Zbontar J, Sodickson DK, Knoll F, Yakubova N, Sriram A, et al. Using Deep Learning to Accelerate Knee MRI at 3T: Results of an Interchangeability Study. AJR Am J Roentgenol. 2020;215(6):1421–1429.
16 Gassenmaier S, Afat S, Nickel D, Mostapha M, Herrmann J, Othman AE. Deep learning-accelerated T2-weighted imaging of the prostate: Reduction of acquisition time and improvement of image quality. Eur J Radiol. 2021;137:109600.
17 Skare S, Sprenger T, Norbeck O, Rydén H, Blomberg L, Avventi E, et al. A 1-minute full brain MR exam using a multicontrast EPI sequence. Magn Reson Med. 2018;79(6):3045–3054. doi:10.1002/mrm.26974
18 Delgado AF, Kits A, Bystam J, Kaijser M, Skorpil M, Sprenger T, et al. Diagnostic performance of a new multicontrast one-minute full brain exam (EPIMix) in neuroradiology: A prospective study. J Magn Reson Imaging. 2019;50(6):1824–1833.

Contact

Bryan Clifford, Ph.D.
Siemens Medical Solutions USA
149 13th St, Suite 2301
Boston, MA 02129
USA
Bryan.Clifford@siemens-healthineers.com

19 Wang D, Deshpande V, Li X, Urgurbil K. Siemens Healthcare GmbH, Regents of the University of Minnesota, assignee. Multiband Slice Accelerated Imaging With Balanced Slice-Selective Gradients. United States patent 9,989,610. June 5, 2018.
20 Cauley SF, Polimeni JR, Bhat H, Wald LL, Setsompop K. Interslice leakage artifact reduction technique for simultaneous multislice acquisitions. Magn Reson Med. 2014;72(1):93–102.
21 Clifford B, Conklin J, Huang SY, Feiweier T, Hosseini Z, Goncalves Filho ALM, et al. An artificial intelligence-accelerated 2-minute multi-shot echo planar imaging protocol for comprehensive high-quality clinical brain imaging. Magn Reson Med. 2022;87(5):2453–2463. Epub 2021 December 31.
22 Pruessmann KP, Weiger M, Börnert P, Boesiger P. Advances in sensitivity encoding with arbitrary k-space trajectories. Magn Reson Med. 2001;46(4):638–651.
23 Hyun CM, Kim HP, Lee SM, Lee S, Seo JK. Deep learning for undersampled MRI reconstruction. Phys Med Biol. 2018;63(13):135007.
24 Wang S, Su Z, Ying L, Peng X, Zhu S, Liang F, et al. ACCELERATING MAGNETIC RESONANCE IMAGING VIA DEEP LEARNING. In: Proc IEEE Int Symp Biomed Imaging. 2016;2016:514–517.
25 Mason A, Rioux J, Clarke SE, Costa A, Schmidt M, Keough V, et al. Comparison of Objective Image Quality Metrics to Expert Radiologists' Scoring of Diagnostic Quality of MR Images. IEEE Trans Med Imaging. 2020;39(4):1064–1072.
26 Muckley MJ, Riemenschneider B, Radmanesh A, Kim S, Jeong G, Ko J, et al. Results of the 2020 fastMRI Challenge for Machine Learning MR Image Reconstruction. IEEE Trans Med Imaging. 2021;40(9):2306–2317.
27 Hosseini Z, Feiweier T, Conklin J, et al. A data-driven method for automatic regularization selection in a hybrid DL-SENSE reconstruction. In: Proc. Intl. Soc. Magn. Reson. Med. 2022:0206.
28 Tabari A, Clifford B, Goncalves Filho ALM, Hosseini Z, Feiweier T, Lo WC, et al. Ultrafast Brain Imaging with Deep Learning Multi-Shot EPI: Preliminary Clinical Evaluation. MAGNETOM Flash. 2021;79(2):66–70.

Speed up stroke care for your patients.

Explore our comprehensive offering for stroke care.

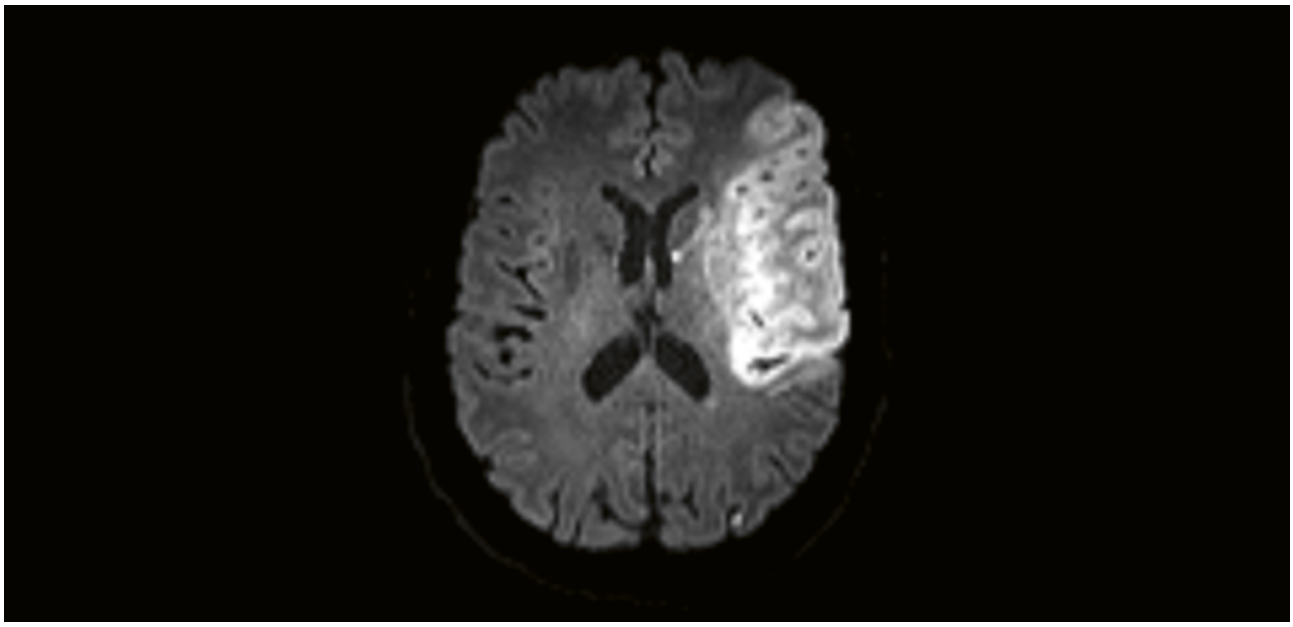

As your partner in stroke management, we keep you ahead of your time. Our advanced technologies let you speed up stroke care and transform care delivery along the entire pathway – from stroke screening and pre-hospital diagnosis and care to in-hospital diagnosis and treatment. Explore our offerings for stroke care!

Optimal treatment across all steps of the clinical pathway is crucial for good patient outcome

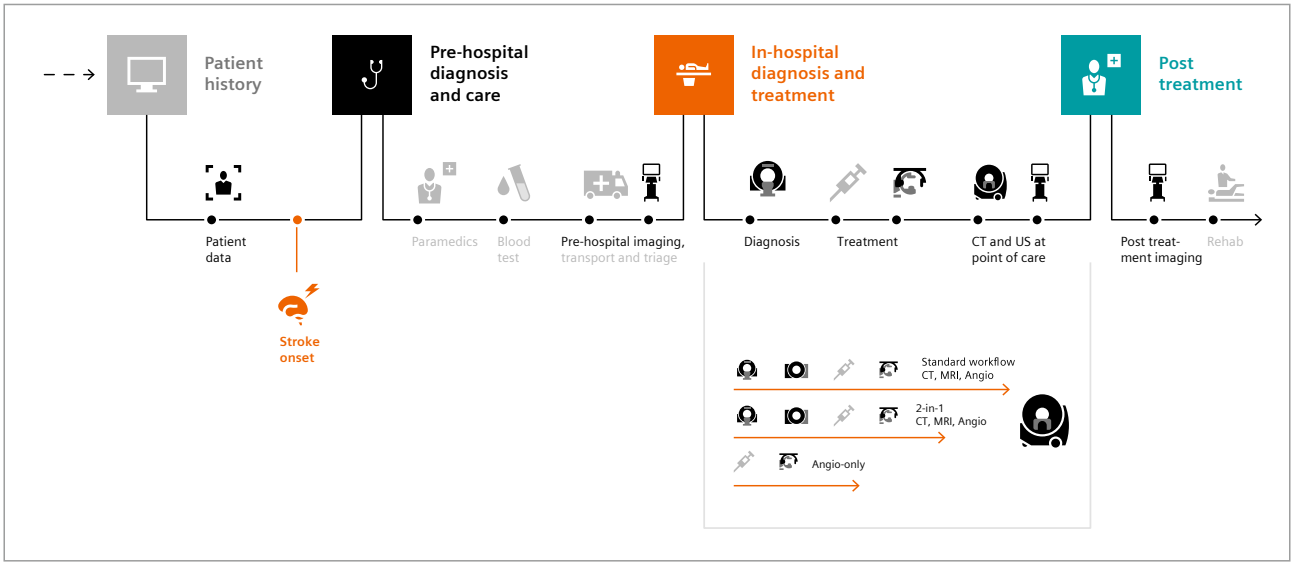

Visit us at

https://www.siemens-healthineers.com/clinical-specialities/neurology/stroke-care

Simultaneous Multi-Slice (Slice Accelerated) Diffusion EPI: Early Experience for Brain Ischemia and Cervical Lymphadenopathy

Val M. Runge, M.D.[1]; Johannes K. Richter, M.D.[2]; Markus Klarhöfer, Ph.D.[3]; Thomas Beck, Ph.D.[4]; Johannes T. Heverhagen, M.D.[1]

[1] Department of Diagnostic, Interventional and Pediatric Radiology, University Hospital of Bern, Inselspital, Bern, Switzerland
[2] Clinics for Neuroradiology, University Hospital Zurich, Switzerland
[3] Siemens Healthcare, Zurich, Switzerland
[4] Siemens Healthcare, Erlangen, Germany

Introduction

In single shot EPI, the entirety of *k*-space is traversed after one shot (excitation). Readout-segmentation acquires *k*-space in multiple shots for reduced TE and encoding time. Real-time reacquisition of unusable shots is also supported. The result is markedly improved image quality, with reduced susceptibility artifact and image blur. The challenge with this approach, termed RESOLVE, is the longer scan time, which scales with the number of readout segments. Here slice acceleration (simultaneous multi-slice) can play a very important role, to reduce scan time, when applied in combination with RESOLVE.

Simultaneous multi-slice (SMS) accelerated diffusion-weighted echo planar imaging employs an innovative acquisition and reconstruction scheme that allows multiple slices to be acquired simultaneously [1-4]. The approach offers a substantial decrease in image acquisition time, or alternatively improved spatial / diffusion resolution. The advent of this technique is analogous to that years ago of 2D multi-slice, and as such may represent one of the major innovations in this decade for MRI with widespread clinical utility. This short article covers briefly the theory behind the approach, advantages and limitations, and applications in the brain and the soft tissues of the neck using clinical cases.

Method

The breadth of capabilities and current limitations with SMS diffusion EPI in brain imaging are illustrated at 3T. In this approach (provided as a works-in-progress software package[1]), multiple slices are acquired simultaneously using blipped-CAIPIRINHA technique with the individual slices then reconstructed using a slice-GRAPPA method. Slice acceleration with axial imaging, as applied, requires a phased array coil with sufficient elements in the z-direction, which in this instance was accomplished by use of a 32-channel head coil.

For slice acceleration, the RF excitation is modified, to excite multiple slices simultaneously, and during readout, phase-blips are applied to shift / alias simultaneously excited slices. Aliased slices are separated during reconstruction using a slice-GRAPPA approach, with a high-quality slice separation requiring an appropriate multi-element coil. SMS acceleration allows more slices per TR or TR to be reduced with the same slice coverage. Potentially there is no SNR loss due to undersampling, and the *g*-factor penalty is reduced by employing gradient-based CAIPIRINHA.

[1] The product is still under development and not commercially available yet. Its future availability cannot be ensured.

Case 1

Slice acceleration with RESOLVE for decreased scan time. The patient presented with both Broca's (motor) and Wernicke's (sensory) aphasia, together with transient weakness of the right hand. A large early subacute infarct is seen in the left middle cerebral artery and watershed territories. With an acceleration factor of 2, the scan time is reduced by 1 minute (from 3:08 to 2:06 min:sec), with no loss in image quality. Indeed, the resultant image has less blur.

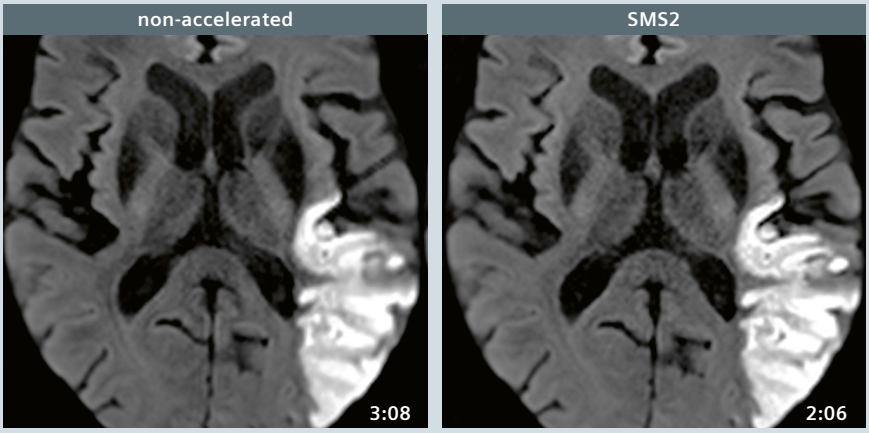

Case 2

Slice acceleration with RESOLVE to achieve a thinner axial section. This is the same patient as illustrated in case 1, but at a higher level showing scattered punctate early subacute infarcts in the cortex and deep white matter of the parietal lobe. By moving to a 2 mm slice (not possible without slice acceleration due to the long scan time), the small pinpoint infarcts that are present are better seen (black arrows), and some revealed for the first time (white arrow). Scan times are given in the lower right hand corner of each image, with complete coverage of the brain in each instance (30 slices with a 4 mm thickness vs. 60 slices with a 2 mm thickness).

For 2D diffusion-weighted imaging (DWI) of the brain, TR is typically ≈ 6000 msec. However a reduction to 3500 does not impact substantially image quality or signal-to-noise ratio (SNR). Making use of the possibility to shorten TR expands the potential of SMS accelerated imaging, whether slice thickness is maintained or reduced. Specifically, SMS acceleration can be used in clinical brain DWI in this manner to either shorten scan time or to allow thinner sections covering the entire brain within a reasonable acquisition time.

Depending upon level of the brain, likely coil dependent, SNR results vary. Near the vertex, SNR was essentially equivalent for all scans. At the level of the lateral ventricles, mild decreases in SNR were seen that could be attributable not only to the decrease in TR and slice thickness, but also to the number of simultaneously excited slices (*g*-factor of the coil). When comparing the standard 4 mm single shot scan, to the SMS acceleration 3, 2 mm, short TR scan, the decrease in SNR was 27%, likely primarily due to the thinner slice.

The combination of the readout segmented approach (RESOLVE) with slice acceleration (SMS RESOLVE) provides images with markedly reduced bulk susceptibility effect as well as image blur, with 2 mm slices through the entire brain, in a relatively short scan time. Alternatively, if the slice thickness is kept at 4 mm – the standard for clinical imaging of the brain at 3T, scan time is reduced by a third, in the approach implemented. Not evaluated, but extremely simple and of substantial clinical value, would be the use of slice acceleration to acquire a higher number of b-values in the same scan time.

Similarly, SMS RESOLVE can be applied in the neck, provided a sufficient number of coil elements are present in the slice direction. Here, with a 3 mm slice thickness, the primary application would be for a reduction in scan time.

Conclusion

The utility of SMS in combination with RESOLVE is demonstrated in cerebral ischemia, by allowing – with equivalent image quality – scan acquisition time to be shortened or slice thickness to be reduced [5]. A reduction in scan time was also demonstrated for imaging of the soft tissues of the neck. SMS RESOLVE with slice acceleration 2 led to a scan time reduction from 3:08 (min:sec) to 2:06, with the reference scan acquisition implemented (in the current works-in-progress package) preventing a true factor of 2 reduction in scan time. Combining an SMS acceleration of 3 with a reduction in slice thickness, 2 mm sections through the entire brain were also demonstrated, with scan time and image quality comparable to the 4 mm single slice RESOLVE diffusion EPI acquisition.

SMS accelerated imaging offers a marked reduction in the time required for data acquisition (scan time). Using this approach, thin section (2 mm) DWI of the entire brain can also be acquired in a scan time and with image quality equivalent to 4 mm imaging with conventional DWI. Thin section imaging brings a marked further improvement in diagnostic image quality to 3T of the brain. This holds true especially for exams in patients with suspected brainstem pathology (a region in which every voxel contains eloquent tracts or nuclei). This new sequence approach is also easily applied in other anatomic areas, with many potential applications [6]. Looking further to the future, SMS accelerated imaging can be extended to additional pulse sequences, specifically TSE T2-weighted imaging.

Case 3

Slice acceleration with RESOLVE – the advantages of a thinner section. Bulk susceptibility artifacts on DWI are further reduced, and small pinpoint lesions with restricted diffusion are better seen. And, as shown, in certain instances small pinpoint lesions can be visualized only on the thinner sections, such as this small cortical infarct (arrow) in the left middle frontal gyrus.

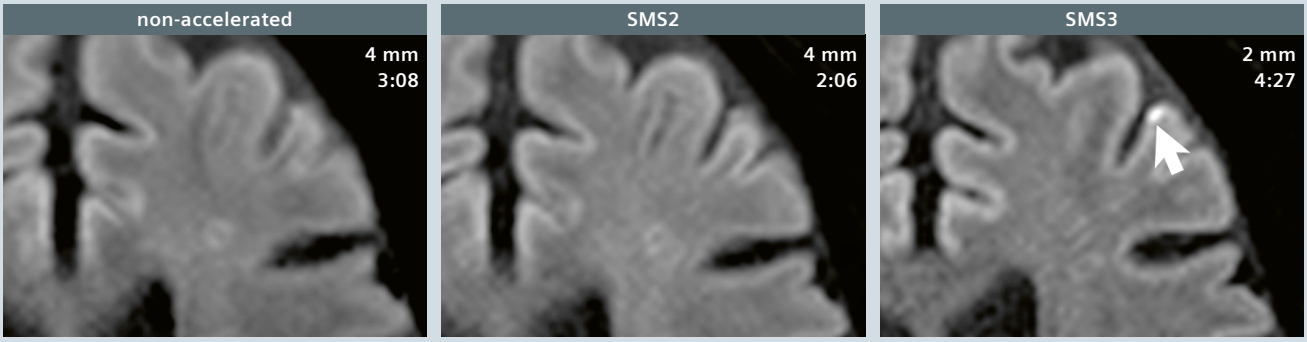

Case 4

Do we have good depiction of this lateral medullary infarct, with single shot imaging (upper row)? The conventional answer would be that the infarct is well delineated, with 4 mm slices acquired at 3T. But no, this is just a misconception, due to limited experience with thinner sections! This small infarct is not nearly as well seen as with 2 mm sections – acquired using slice acceleration (lower row), where the infarct is more sharply defined on each section and we have an additional slice (in between). The patient, an 87-year-old woman, presented one day prior to the MR with dizziness, nausea and vomiting, and left facial paralysis.

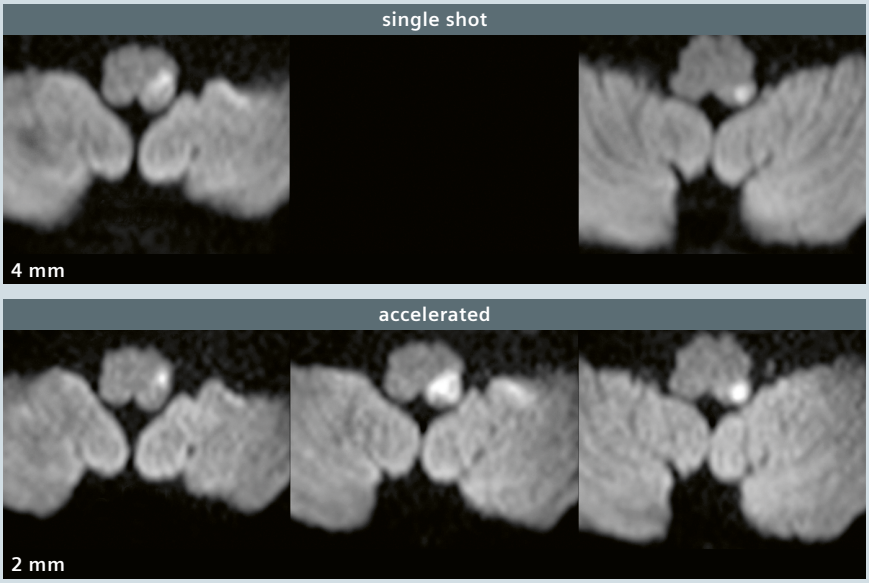

Case 5

In this example, the patient (with multiple punctate, acute, left middle cerebral artery distribution infarcts) was combative and moved throughout the exam despite sedation, degrading image quality. Motion artifact is greatest on the readout segmented DWI exam, due both to the long scan duration (3:26 min:sec) and the acquisition scheme, and least on the 2 mm slice accelerated scan. This 67-year-old patient presented one day prior to the MR with global aphasia, a right facial palsy and – on other imaging studies – a distal M1 segment occlusion.

Case 6

Axial (part 1, 6A-C) and sagittal (part 2, 6D, E) soft tissue neck images from a normal volunteer are presented, without and with slice acceleration. In part 1, a single-shot (ss) DWI exam is compared to RESOLVE acquired without and with slice acceleration. Note the artifactual foreshortening in the AP dimension on the ss exam, which leads to a lymph node (arrow) that is anterior to the submandibular gland on the left being projected over the gland. On the RESOLVE images, there is no anatomic distortion, with the effective spatial resolution also improved due to the absence of the artifactual blurring present in the ss exam (and inherent to this technique). The use of slice acceleration allowed the RESOLVE sequence to be obtained in a very similar scan time as with the ss DWI, 2:07 vs 1:50 min:sec. In part 2, off-midline sagittal RESOLVE diffusion-weighted images are presented. Of intermediate signal intensity is a very small part of the submandibular gland with a high signal intensity small lymph node immediately anteriorly (in the middle of image), with a portion of the parotid gland seen in the more superior portion of the image. Depiction of the multiple scattered, high signal intensity, normal lymph nodes and SNR are equivalent for the two scans, with slice acceleration reducing scan time by nearly a factor of 2 (from 3:44 to 2:07 min:sec). Images were acquired with the Head/Neck 64-channel coil.

6A single shot

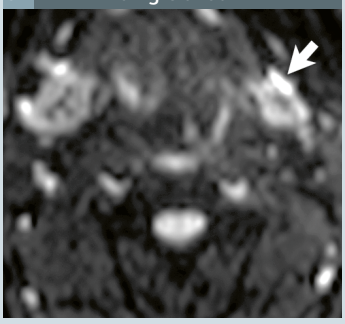

6B readout segmented

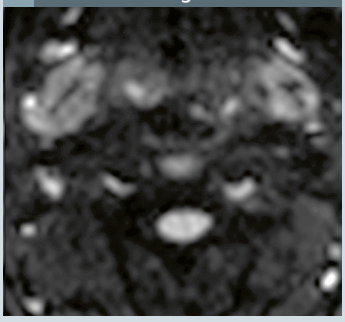

6C readout segmented, SMS2

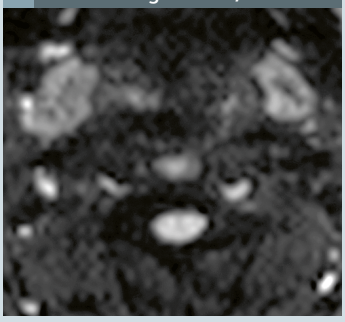

6D non-accelerated

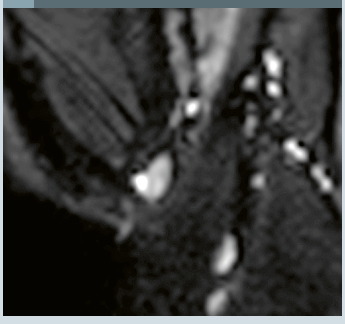

6E SMS2

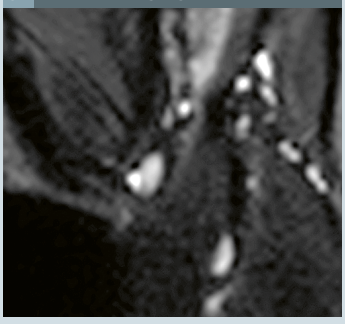

Acknowledgement

All images were acquired at 3T on a MAGNETOM Skyra MR system.

References

1 Larkman DJ, Hajnal JV, Herlihy AH, et al. Use of multicoil arrays for separation of signal from multiple slices simultaneously excited. J Magn Reson Imaging. 2001;13(2):313-7.

2 Setsompop K, Gagoski BA, Polimeni JR, et al. Blipped-controlled aliasing in parallel imaging for simultaneous multislice echo planar imaging with reduced g-factor penalty. Magn Reson Med. 2012;67(5):1210-24.

3 Frost R, Jezzard P, Douaud G, et al. Scan time reduction for readout-segmented EPI using simultaneous multislice acceleration: Diffusion-weighted imaging at 3 and 7 Tesla. Magn Reson Med. 2015;74:136-49.

4 Poser BA, Anderson RJ, Guerin B, et al. Simultaneous multislice excitation by parallel transmission. Magn Reson Med. 2014;71(4):1416-27.

5 Runge VM, Aoki S, Bradley WG, Jr., et al. Magnetic Resonance Imaging and Computed Tomography of the Brain-50 Years of Innovation, With a Focus on the Future. Invest Radiol. 2015;50(9):551-6.

6 Filli L, Piccirelli M, Kenkel D, et al. Simultaneous Multislice Echo Planar Imaging With Blipped Controlled Aliasing in Parallel Imaging Results in Higher Acceleration: A Promising Technique for Accelerated Diffusion Tensor Imaging of Skeletal Muscle. Invest Radiol. 2015;50(7):456-63.

Contact

Val M. Runge, M.D.
Editor-in-Chief, Investigative Radiology
Department of Diagnostic,
Interventional and Pediatric Radiology
University Hospital of Bern, Inselspital
Bern, Switzerland
ValMurray.Runge@insel.ch

On account of certain regional limitations of sales rights and service availability, we cannot guarantee that all products included in this brochure are available through the Siemens sales organization worldwide. Availability and packaging may vary by country and is subject to change without prior notice. Some/All of the features and products described herein may not be available in the United States.

The information in this document contains general technical descriptions of specifications and options as well as standard and optional features which do not always have to be present in individual cases, and which may not be commercially available in all countries.

Due to regulatory reasons their future availability cannot be guaranteed. Please contact your local Siemens organization for further details.

Siemens reserves the right to modify the design, packaging, specifications, and options described herein without prior notice. Please contact your local Siemens sales representative for the most current information.

Note: Any technical data contained in this document may vary within defined tolerances. Original images always lose a certain amount of detail when reproduced.

Siemens Healthineers Headquarters
Siemens Healthcare GmbH
Henkestr. 127
91052 Erlangen, Germany
Phone: +49 9131 84-0
siemens-healthineers.com

Published by Siemens Healthcare GmbH · Order No. A91MR-1000-138C-7600 · Printed in Germany · 13288 0323 ·

siemens-healthineers.com/magnetom-world